# CONCEPTS FOR A THEORETICAL AND EXPERIMENTAL

## STUDY OF LIFTING ROTOR RANDOM

## LOADS AND VIBRATIONS

### (Experiments with Progressing/Regressing
### Forced Rotor Flapping Modes)

#### Phase VI-B Report under Contract NAS2-4151

by

## Kurt H. Hohenemser

and

## S. T. Crews

## Department of Mechanical and
## Aerospace Engineering

AUG 1972
RECEIVED
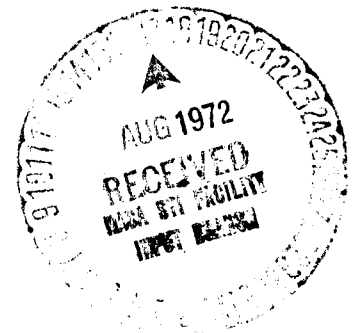
## Washington University
## School of Engineering and Applied Science
## St. Louis, Missouri

### June, 1972

72p

# N O T I C E

CONCEPTS FOR A THEORETICAL AND EXPERIMENTAL

STUDY OF LIFTING ROTOR RANDOM

LOADS AND VIBRATIONS

(Experiments with Progressing/Regressing
Forced Rotor Flapping Modes)

Phase VI-B Report under Contract NAS2-4151

Prepared for the Ames Directorate, AMRDL,
at Ames Research Center, Moffett Field, California

by _____

Kurt H. Hohenemser

and _____

S. T. Crews

## Scope of Contract NAS2-4151

Work under Contract NAS2-4151 started on February 1, 1967. Phase I Report of September 1967 develops analytical concepts for a random loads and vibration analysis of lifting rotors. Phase II Report of August 1968 presents a perturbation solution method for random blade flapping. Phase III Report of June 1969 develops a more general method to include high rotor advance ratios and makes use of a specific atmospheric turbulence model. Phase IV Report of June 1970 extends the method to the computation of threshold crossing statistics for random blade flapping and introduces non-uniformity of the vertical turbulence velocity in the longitudinal direction. Phase V-A Report of June 1971 treats the effects of torsional blade flexibility on single blade random gust response statistics. Phase V-B Report of June 1971 presents a multiblade coordinate analysis of coupled blade dynamic stability and random response, studying various gust alleviation methods. Phase V-C Report of June 1971 describes the development of experimental methods of substantiating the random loads and vibration analysis.

During FY 1972 the work was extended in two directions, resulting in two separate Phase VI reports. Phase VI-A Report covers three refinements of the preceding analysis. The effects of blade torsion on dynamic stability and random

response has been analyzed beyond Phase V-A Report, adding new insights into this subject matter. The effects of blade flap bending flexibility on rotor stability and random response have been studied leading to a simple method of correcting the rigid blade analysis. Finally the effects of rotor support flexibility have been analyzed, solving the problem of whirl flutter in high advance ratio oblique flow. Phase VI-B Report covers the experimental work performed in FY 1972 to substantiate the analysis. The work summarized in Phase VI-A and Phase VI-B Reports was performed under Modification 7 to subject contract, which covers also FY 1973. The scope of the work planned for FY 1973 is to further remove limitations to the present analytical model and at the same time to simplify the methods of analysis, and to conduct further tests in support of the analysis.

The following is a list of publications sponsored under subject research contract issued to date.

1. Gaonkar, G. H. and Hohenemser, K. H., "Flapping Response of Lifting Rotor Blades to Atmospheric Turbulence", Journal of Aircraft, Vol. 6, No. 6, Nov.-Dec. 1969, pp. 496-503. First presented as AIAA Paper 69-206 at the AIAA/AHS VTOL Meeting, Atlanta, Georgia, February 1969.

2. Gaonkar, G. H. and Hohenemser, K. H., "Stochastic Properties of Turbulence Excited Rotor Blade Vibrations", AIAA Journal, Vol. 9, No. 3, March 1971, pp. 419-424. First presented as AIAA Paper 70-548 at the AIAA Atmospheric Flight Mechanics Conference, Tullahoma, Tennessee, May 1970.

3. Gaonkar, G. H. and Hohenemser, K. H., "Comparison of Two Stochastic Models for Threshold Crossing Studies of Rotor Blade Flapping Vibrations", Presented as AIAA Paper 71-389 at the AIAA/ASME 12th Structures Conference, Anaheim, California, April 1971.

4. Gaonkar, G. H. and Hohenemser, K. H., "An Advanced Stochastic Model for Threshold Crossing Studies of Rotor Blade Vibrations", AIAA Journal, Vol. 10, No. 6, July 1972.

5. Yin, S. K. and Hohenemser, K. H., "The Method of Multi-blade Coordinates in the Linear Analysis of Lifting Rotor Dynamic Stability and Gust Response", Presented as AHS Preprint No. 512 at the 27th Annual National Forum of the AHS, Washington, D. C., May 1971.

6. Hohenemser, K. H. and Yin, S. K., "Some Applications of the Method of Multiblade Coordinates", Journal of the American Helicopter Society, Vol. 17, No. 3, July 1972.

# CONCEPTS FOR A THEORETICAL AND EXPERIMENTAL STUDY OF LIFTING ROTOR RANDOM LOADS AND VIBRATIONS

### Phase VI-B

### (Experiments with Progressing/Regressing Forced Rotor Flapping Modes)

by

Kurt H. Hohenemser
and
S. T. Crews

Washington University
St. Louis, Missouri

## Abstract

A two bladed 16 inch hingeless rotor model was built and tested outside and inside a 24 by 24 inch wind tunnel test section at collective pitch settings up to 5° and rotor advance ratios up to .4. The rotor model has a simple excentric mechanism to provide progressing or regressing cyclic pitch excitation. The flapping responses were compared to analytically determined responses which included flap-bending elasticity but excluded rotor wake effects. Substantial systematic deviations of the measured responses from the computed responses were found, which were interpreted as the effects of interaction of the blades with a rotating asymmetrical wake.

# CONCEPTS FOR A THEORETICAL AND EXPERIMENTAL

## STUDY OF LIFTING ROTOR RANDOM

## LOADS AND VIBRATIONS

### Phase VI-B

### (Experiments with Progressing/Regressing Forced Rotor Flapping Modes)

## Nomenclature

| | |
|---|---|
| a | lift slope (5.6) |
| c | blade chord (uniform) |
| $F_1(t)$, $F_2(t)$ | real functions with period $2\pi$ |
| $F_{1s}$, $F_{2s}$, $F_{1c}$, $F_{2c}$ | Fourier coefficients of terms sin t and cos t |
| $G_1(t)$, $G_2(t)$ | real functions with period $2\pi$ |
| $H_1(t)$, $H_2(t)$ | real functions with period larger than $2\pi$ |
| I | blade moment of inertia about rotor center |
| M | blade flap bending moment per inch of tip deflection in first bending mode |
| $M_{aer}$ | moment of all aerodynamic vertical loads about rotor center |
| $M_s$ | flap bending moment at strain gauge |
| P | blade flap bending natural frequency with time unit $1/\Omega$ |
| R | rotor radius |
| t | nondimensional time, time unit $1/\Omega$ |
| $\beta$ | blade up flapping angle, defined by line through rotor center and first mode deflection at .66R |
| $\beta_I$, $\beta_{II}$ | forward and left rotor tilt respectively |
| $\beta_o$ | coning angle |
| $\beta_s$, $\beta_c$ | flapping responses to pitch inputs sin $t(1\pm\omega)$ and cos $t(1\pm\omega)$ |
| $\gamma = \rho a c R^4/I$ | lock inertia number |
| $\psi_I$, $\psi_{II}$ | phase differences between responses $\beta_I$, $\beta_{II}$ and inputs $\Theta_I$, $\Theta_{II}$ |
| $\mu$ | rotor advance ratio |

$\Omega$         rotor angular speed

$\omega$         nondimensional circular frequency of progression or regression in non-rotating frame of reference

$\Theta$         blade feathering amplitude

$\Theta_I, \Theta_{II}$         forward and left cyclic pitch

$\Theta_o$         collective pitch angle

## Introduction

In the substall regime relatively few efforts have been
made to introduce unsteady aerodynamics to lifting rotor
analysis.  The classical work by Loewy[1] represents an exten-
sion of the Theodorsen and Küssner theory of oscillating
airfoils in plane flow to the lifting rotor at zero advance
ratio and predicts an appreciable reduction in the aerodyna-
mic damping of flap-bending modes in regions where the flap-
bending frequency is an integral multiple of the rotation
frequency.  Model tests by Daughaday et al[2] have shown a
remarkable agreement of the Loewy theory with test results.
The Loewy effect is, however, only substantial at low rotor
lift and is negligible at collective pitch settings of 4°
and above.  Shipman and Wood[3] have extended Loewy's theory
to forward flight conditions.  In both the original and the
extended theory a uniform wake is assumed in which the free
vorticity shed from the oscillating airfoil is embedded.  The
theory is, therefore, only applicable to relatively high
frequency small amplitude coupled blade torsional and flap
bending oscillations which do not appreciably affect the
mean rotor wake.

There is an extensive literature on rotor wakes, both
theoretical and experimental.  An example of the early theo-
retical work is Miller[4] who derived the wake from the effects
of trailing vortices due to spanwise changes in blade

circulation, and shed vorticity due to timewise changes of blade circulation. An example of early experimental work is Castles and DeLeeuw[5] whose results were used by Harris[6] to explain the large sidewise flapping of articulated rotors at low advance ratio. Recently Landgrebe[7] presented an experimental study of symmetrical rotor wakes in hovering.

The effects of steady wake asymmetries have attracted considerable attention in studies of hingeless rotors, where they were shown to be responsible for deficiencies in control effectiveness[8] and for changes in static derivatives not only at low but also at high advance ratio.[9] All of this work pertained to the rotor wake in steady lifting rotor conditions. The only work from which some limited conclusions on unsteady wake effects can be drawn is a recent study on dynamic derivatives of hingeless rotors conducted at AAMRDL Ames with a 7.5 ft. diameter 4 bladed hingeless rotor model of .127 blade solidity.[10] The conditions tested were for a low collective pitch setting. The model flapping frequencies were higher than would be practical for a full scale rotor. The experimental results were compared with analytical dynamic derivatives obtained without considering rotor wake effects and without considering elastic blade flap bending effects. The agreement is good for the hub moment from cyclic pitch at .8 advance ratio and a flap bending natural frequency of p = 1.56. The agreement is not

very good for the hub moment from collective pitch at .40 advance ratio and a flap bending natural frequency of p = 1.33. No other comparisons are shown. From Reference 9 it is clear that even for steady rotor conditions sizeable flap bending effects and wake effects must be expected at .8 advance ratio, so that the agreement with the rigid blade theory without wake is probably caused by compensating influences of the neglected effects.

While the AAMRDL tests used single axis excitation of the cyclic controls, the tests presented here used progressing and regressing modes of cyclic control excitation. One reason for selecting such excitation was the desire for simplicity of the test apparatus, which did not require oscillating actuators but which used instead actuation of the cyclic pitch by an excentric. However, there also is a more basic reason for selecting progressing and regressing excitation rather than single axis excitation of the cyclic control. Unstable rotor modes, because of interblade coupling, occur in the form of advancing and regressing blade flapping.[11] It is, therefore, of particular interest to find out what unsteady wake interactions exist for such modes.

## A Qualitative Model of Unsteady Wake Blade Interaction

We consider a progressing blade flapping excitation at zero rotor advance ratio. The blade is assumed to be rigid and to flap about the rotor center where it is elastically restrained. In the absence of a wake, assuming uniform blade chord and ignoring blade tip and root losses, the equation of forced blade flapping through harmonic pitch excitation is in a rotating frame of reference

$$\ddot{\beta} + (\gamma/8)\,\dot{\beta} + P^2\beta = \Theta(\gamma/8)\exp\,it(1-\omega) \qquad (1)$$

The period of excitation and response is $2\pi/(1-\omega)$. As shown in Fig. 1a the maximum of blade flapping progresses in the direction of rotation. The aerodynamic up moment on the blade at the instance of maximum up flapping is equal to the elastic plus centrifugal plus inertial moment

$$M_{aer}/I = \beta(P^2 - (1-\omega)^2) \qquad (2)$$

If $P > (1-\omega)$ the aerodynamic moment on the blade is associated with a downwash as indicated by the arrows in Fig. 1a at the left hand maximum of $\beta$. This downwash area, though attenuated, is encountered again by the blade after the time interval $t = 2\pi$. At this time the blade has not yet reached its maximum up flapping position and is still on its way up. The downwash, therefore, produces a moment on the blade with the same sign as the aerodynamic damping moment. One can also express the unsteady wake geometry by stating that in a progressing flapping mode the location of maximum downwash leads

the location of maximum up flapping, while both rotate in
the same direction as the blade. The effect of this lead
is equivalent to an increased blade aerodynamic damping.

We now consider a regressing blade flapping excitation
with a period of excitation and response in a rotating frame
of reference of $2\pi/(1+\omega)$. As shown in Fig. 1b the maximum
of blade flapping regresses opposite to the direction of
rotation. We first assume $P > (1+\omega)$. The aerodynamic moment

$$M_{aer}/I = \beta(P^2 - (1+\omega)^2) \tag{3}$$

is then upward for positive $\beta$ with an associated downwash
as indicated by the arrows in Fig. 1b at the left hand maxi-
mum of $\beta$. This downwash area though attenuated is encoun-
tered again by the blade after the time interval $t = 2\pi$.
At this time the blade is beyond its maximum up position and
on its way down. The downwash, therefore produces a moment
on the blade with the opposite sign as the aerodynamic
damping moment.

Finally, if $P < (1+\omega)$, the aerodynamic moment of Eq. (3)
is downward for positive $\beta$ with an associated upwash as
indicated by Fig. 1c. The upwash, though attenuated, is
encountered by the blade again at $t = 2\pi$, when it is on its
way down and produces a moment on the blade with the same
sign as the aerodynamic damping moment. When the blade is
in resonance, $P = 1+\omega$, no aerodynamic moment acts on the
blade, see Eq. (3), and no dynamic wake should be produced.
One would then expect from this qualitative model that as

compared to an analysis with neglected unsteady wake a pro-
gressing flapping mode will always cause increased blade
damping, a regressing flapping mode will cause decreased
blade damping below resonance excitation and increased blade
damping above resonance excitation, while at resonance no
unsteady wake effect should be encountered.

For a freely flapping blade hinged without elastic
restraint at the rotor center, the resonance occurs at $\omega = 0$.
In this case both progressing and regressing flapping modes
would have more damping than would exist without the unsteady
wake.  It should be remembered that an increase in blade
damping causes a decrease in airframe damping and vice versa.
Except in the case of Fig. 1b which can occur only for hinge-
less rotors or rotors with hinge offset, the effect of the
unsteady wake is to decrease airframe damping from the rotor
in both progressing and regressing tilting modes, unless
the modes occur with the blade natural frequency.  The unsteady
wake effect may, therefore, be of importance in conditions
of whirl flutter or of air resonance caused by in plane blade
motions.  Control dynamics may also be affected by the unsteady
wake.

## The Rotor Model

The hingeless rotor model is two bladed with 16 inch
diameter and 1 inch blade chord. Fig. 2 shows a schematic
of the hub and blade attachment and the cyclic pitch excita-
tion mechanism. Each blade is connected with a flexure F
to a center feathering shaft S which is feathered with the
help of a bending spring B from an excentric E driven by the
internal shaft I. The feathering shaft S is split into a
left and right half clamped together by bolts not shown in
the schematic. An adjustment of the pitch angles of the
blades with respect to each other and with respect to the
feathering spring B is accomplished by loosening the bolts
and rotating the two halves of the feathering shaft into pro-
per position. Due to the absence of any push pull rods and
of any bearing except for the two bearings supporting the
feathering shaft $S_1$ the pitch control mechanism, in spite
of the small scale, is very stiff and free of play. A
feathering amplitude of $\pm 1.5°$ was used for the tests. The
excentric shaft is driven from the rotor shaft by a set of
exchangeable gears, whereby the excentric shaft can rotate
with $0, \pm .05, \pm .1, \pm .2, \pm .4, \pm .6, \pm 8$ times rotor speed.
The gear set allows adjustments of the phase angle between
excentric shaft and rotor shaft. Both shafts carry magnetic
pick-ups to define the azimuth angle of each shaft. One
blade attachment flexure is strain gauged for blade flap

bending, the other for blade torsion.  Fig. 3 shows a schema-
tic side view of the rotor as installed in the wind tunnel
test section.  The installation is aerodynamically very clean.

The open return wind tunnel has a 24 by 24 inch test
section.  For such a small tunnel the flow is remarkably
uniform.  To avoid flow breakdown at low tunnel speed, the
lowest rotor advance ratio tested was chosen to be .2.  The
condition of zero advance ratio was tested outside the wind
tunnel.

When the rotor shaft is turning and the excentric shaft
is fixed, steady cyclic pitch is applied.  By proper posi-
tioning of the excentric shaft one obtains either longitu-
dinal or lateral cyclic pitch input.  When turning the
excentric shaft in the direction of rotor rotation, one
obtains a progressing flapping mode characterized in the
rotating reference system by a reduced flapping frequency
$1-\omega$, see Fig. 1a.  When turning the excentric shaft opposite
to the rotor rotation, one obtains a regressing flapping
mode characterized in the rotating frame of reference by an
increased flapping frequency $1+\omega$, see Fig. 1b and 1c.  In
order to get complete response data it is necessary to excite
the control both in the cosine and sine mode which can be
done by properly phasing the excentric shaft with respect
to the rotor shaft.

## Table 1

## Model Characteristics

| | |
|---|---|
| Rotor diameter, inch | 16 |
| Blade chord, inch | 1 |
| Airfoil | 0012 |
| Center of flexure to rotor center, inch | .7 |
| Number of blades | 2 |
| Rotor solidity | .080 |
| First flap bending frequency, cps | 11.6 at 0 rps |
| | 24.3 at 20.3 rps |
| Second flap bending frequency, cps | 152 at 0 rps |
| | 161 at 20.3 rps |
| First torsional frequency, cps | 180 at 0 rps |
| | 184 at 20.3 rps |
| First chordwise frequency, cps | 200 |
| Blade Lock number ($\alpha$ = 5.6) | 4.0 |

Table 1 gives some data on the rotor model. The blade natural frequencies at zero rotor speed were determined experimentally by exciting the blade with a magnetic exciter and by determining electronically the frequency for 90° phase shift between response and excitation. The experimental natural frequencies were checked analytically and the unknown blade bending stiffness was adjusted until complete

agreement between test and analysis for both first and second bending frequencies was achieved. The frequencies, mode shapes and flap bending moments, non-rotating and rotating, were determined by a finite element analysis, whereby the blade was divided into 20 elements of unequal length. A small length of the elements was required in the region of the flexure because of the high bending curvature in this region. The blade mass and stiffness distribution is uniform except in the region of the flexure. The blade torsional frequencies were determined experimentally by applying an external axial force equivalent to the centrifugal force to the blade. The data thus obtained reflect the stiffening effect of the centrifugal force on the flexure but not the so called tennis racket effect, which will slightly increase the torsional frequencies. The chordwise blade frequency was determined analytically. Fig. 4 shows the computed bending moment of the first mode per unit tip deflection over the inner portion of the blade for 0 and 20.3 rotor rps. By coincidence the curves intersect at the center of the flap bending strain gauge, so that the value .41 inch lbs. per inch tip deflection can be used independent of rotor rps. This value was checked experimentally by loading the blade at the .7 radius station with the transverse and axial loads corresponding to one inch tip deflection at the various rotor rps values.

For both analysis and experiment the flapping angle $\beta$ is arbitrarily defined by the straight line from the rotor center to the first mode deflection at .66 radius, see Fig. 5. One inch tip deflection then represents 6.6° of flapping angle, so that the flap bending moment at the strain gauge per degree of flapping angle is

$$M_s/\beta = .062 \text{ in lbs/°}$$

Since the strain gauge signal is calibrated in terms of volts per inch lb. flap bending moment, this signal is proportional to the flapping angle $\beta$.

## Method of Data Acquisition and Processing

An effort was made to conduct the tests within the linear range of the lift-angle of attack relationship. The stall angle of attack at the average Reynolds number of the .7 R blade station is about 7°. The coning angle-pitch angle relationship for zero advance ratio, measured outside the wind tunnel is shown in Fig. 6. Blade stall sets in at about 11° blade collective pitch angle.

The separation of the frequency response from the trim response is performed in the following way. The equations are written for the progressive mode. The cyclic pitch

excitation in the rotating frame of reference is

$$\Theta = |\Theta| \exp it(1-\omega) = |\Theta| [\cos t + i \sin t] \exp(-i\omega t) \quad (4)$$

Separate tests are used for the real and imaginary portion.

Excitation: $\quad |\Theta| \cos t(1-\omega) \quad ; \quad |\Theta| \sin t(1-\omega)$

Response: $\qquad \beta_c(t) \qquad ; \qquad \beta_s(t)$ $\qquad\qquad (5)$

where $\quad \beta = \beta_c + i \beta_s \qquad\qquad\qquad\qquad (6)$

The response is of the form

$$\beta = [F_1(t) + i F_2(t)]\exp(-i\omega t) + G_1(t) + i G_2(t) \quad (7)$$

where $F_1(t)$, $F_2(t)$, $G_1(t)$, $G_2(t)$ are real functions with

period $2\pi$, the first two arising from the response to the

pitch excitation, the last two from the response to the

rotor trim condition. Eq. (7) is multiplied by $\exp(i\omega t)$:

$$\beta \exp(i\omega t) = F_1(t) + iF_2(t) + [G_1(t) + iG_2(t)]\exp(i\omega t) \quad (8)$$

This expression will contain harmonics with frequencies

$$\omega, \; 1-\omega, \; 1, \; 1+\omega, \; 2-\omega, \; 2, \; 2+\omega, \; \ldots$$

Due to the gearing between rotor shaft and excentric shaft

all these frequencies are integer multiples of a basic fre-

quency. For example, with basic frequency $\omega_o = .2$ and $\omega = .4$

we have

$$.4, \; .6, \; 1, \; 1.4, \; 1.6, \; 2, \; 2.4, \; \ldots$$

The frequency response includes the harmonics 1, 2, 3, . . .

The trim response the harmonics $\omega$, $1-\omega$, $1+\omega$, $2-\omega$, $2+\omega$, . . .

and it is thus simple by Fourier analysis to separate the

frequency response from the trim response. The Fourier

coefficients for the frequency 1 represent rotor tilting,

the Fourier coefficients for frequencies 2, 3, . . .

represent tip path warping.

Writing Eq. (8) in the form

$$(\beta_c + i\beta_s) \exp(i\omega t) = H_1(t) + iH_2(t) \qquad (9)$$

we have

$$H_1(t) = \beta_c \cos \omega t - \beta_s \sin \omega t \qquad (10)$$

$$H_2(t) = \beta_c \sin \omega t + \beta_s \cos \omega t$$

If $2\pi/\omega_0$ is the period of $H_1(t)$ and $H_2(t)$ the Fourier

coefficients for the frequency 1 which represent rotor

tilting are

$$F_{1c} = (\omega_0/\pi) \int_0^{2\pi/\omega_0} H_1(t) \cos t \, dt$$

$$F_{2c} = (\omega_0/\pi) \int_0^{2\pi/\omega_0} H_2(t) \cos t \, dt$$

$$\left. \begin{array}{l} \\ \\ \\ \end{array} \right\} \qquad (11)$$

$$F_{1s} = (\omega_0/\pi) \int_0^{2\pi/\omega_0} H_1(t) \sin t \, dt$$

$$F_{2s} = (\omega_0/\pi) \int_0^{2\pi/\omega_0} H_2(t) \sin t \, dt$$

In terms of forward and left tilt $\beta_I$ and $\beta_{II}$ the response

is given by

$$\beta_I = (F_{1c} + i \, F_{2c}) \exp(-i\omega t) \qquad (12)$$

$$\beta_{II} = (F_{1s} + i \, F_{2s}) \exp(-i\omega t)$$

In terms of forward and left cyclic pitch $\Theta_I$ and $\Theta_{II}$ Eq. (4)

is equivalent to

$$\Theta_I = -i \, |\Theta| \exp(-i\omega t) \qquad (13)$$

$$\Theta_{II} = |\Theta| \exp(-i\omega t)$$

Thus we obtain the amplitude ratios

$$|\beta_I|/|\Theta| = (F_{1c}^2 + F_{2c}^2)^{1/2}/|\Theta|$$

$$(14)$$

$$|\beta_{II}|/|\Theta| = (F_{1s}^2 + F_{2s}^2)^{1/2}/|\Theta|$$

and the phase differences

$$\psi_I = \arg \beta_I - \arg \Theta_I = \arg (F_{1c} + iF_{2c}) + \pi/2$$

$$(15)$$

$$\psi_{II} = \arg \beta_{II} - \arg \Theta_{II} = \arg (F_{1s} + iF_{2s})$$

Eqs. (14) and (15) describe the results in a space fixed reference system. All equations are written for progressing excitation. For regressing excitation the sign of $\omega$ must be reversed everywhere. While in the following only the rotor tilting response according to Eqs. (14) and (15) will be presented, the higher harmonic contents of $F_1(t)$ and $F_2(t)$ with frequencies 2, 3, . . . is available and represents warping of the tip path.

The preceding method of separating the control responses from the trim responses does not work for steady states with $\omega = 0$, since both cyclic control inputs and trim inputs lead to periodic responses with harmonic contents 1, 2, 3, . . . In the steady cases one must measure both the trim and control response and subtract the first from the second. Obtaining the dynamic control derivatives is, therefore, simpler than obtaining the static control derivatives. The flapping response as well

as the phases of the response and the excitation were recorded on magnetic tape which was then processed on a PDP-12 analog-digital converter and computer according to the preceding method.

## Discussion of Results

Figs. 7 to 14 show comparisons of computed and measured values for rotor tilting amplitudes $|\beta_I|$, $|\beta_{II}|$ and for the associated phase angles $\psi_I$, $\psi_{II}$. Solid lines are from analysis, dash lines from test. All data have been obtained with 1.5° cyclic pitch amplitude excitation, though the response amplitudes are shown per unit cyclic pitch amplitude. The bulk of the data is for a blade natural frequency of P = 1.20 obtained at 20.3 rotor rps, and for a collective pitch setting of $\theta_o$ = 5°. However, Fig. 13 is for 2° collective pitch setting at $\mu$ = 0 with P = 1.20. In all conditions the rotor shaft was perpendicular to the flow direction. Within the framework of the linear analysis,[*] which included flap bending flexibility in the first mode, see Fig. 5, but which excluded wake effects, neither shaft angle of attack nor collective pitch setting have an effect on the flapping response from progressing or regressing cyclic pitch input. For $\mu$ = 0 there is no difference between $|\beta_I|$ and $|\beta_{II}|$ and between $\psi_I$ and $\psi_{II}$. For $\mu \neq 0$

[*]The analysis was performed by Dr. S. K. Yin.

increasing differences occur.

The Figures 7 to 14 show substantial systematic devia-
tions of the test results from the analytical results,
essentially in accordance with the preceding qualitative
unsteady wake model. At resonance for $\omega = P - 1$, analysis
and test results agree best as they should. For regressing
excitation with $\omega > (P-1)$ and for progressing excitation
the flapping response is lower than analytically predicted,
for regressing excitation and $\omega < (P-1)$ there is a region
of higher response than predicted. The phase curves also
show systematic deviations from the analytical curves. The
unsteady wake effects diminish with increasing advance
ratio and with increasing collective pitch.

## Conclusion

1. Progressing and regressing rotor flapping modes can be
   easily excited with a very simple two bladed rotor
   model which has no bearings in the hub or control
   system except for two bearings and an excentric for
   blade feathering.

2. Rotor model tests conducted at zero shaft angle have
   revealed substantial systematic deviations from the
   results of a conventional analysis, in agreement with
   a qualitative unsteady wake model.

3. The unsteady wake effects appear to be largest at zero

advance ratio and low collective pitch setting, but contrary to the Loewy unsteady flow phenomenon, the unsteady wake from progressing/regressing flapping remains quite influential at non-zero advance ratio and at higher collective pitch setting.

4. A more complete parametric study of the unsteady wake from progressing/regressing flapping should include effects of flapping frequency, of exciting amplitude, of blade number and solidity, of ground effect, of tip configuration, of rotor angle of attack, of higher advance ratios, etc. A wake flow survey is also required to substantiate and quantify the qualitative unsteady wake model described herein.

## References

1.  Loewy, R. G., "A Two Dimensional Approach to the Unsteady
    Aerodynamics of Rotary Wings", Journal of Aerospace
    Sciences, Vol. 24, 1957, pp. 82-98.

2.  Daughaday, H., DuWaldt, F. and Gates, C., "Investigation
    of Helicopter Blade Flutter and Load Amplification",
    Journal of American Helicopter Society, Vol. 2, No. 3,
    July 1957, pp. 27-45.

3.  Shipman, K. W. and Wood, R. R., "A Theoretical Method
    for Rotor Blade Flutter in Forward Flight", 26th Annual
    National Forum of the American Helicopter Society,
    Preprint 410, June 1970.

4.  Miller, R. H., "On the Computation of Airloads Acting
    on Rotor Blades in Forward Flight", Journal of American
    Helicopter Society, Vol. 7, No. 2, April 1962, pp. 56-66.

5.  Castles, W. and DeLeeuw, J. H., "The Normal Component of
    the Induced-Velocity in the Vicinity of Lifting Rotors
    and Some Examples of Its Applications", NACA TN 2912, 1953.

6.  Harris, F. D., "Articulated Rotor Blade Flapping Motion
    at Low Advance Ratio", Journal of American Helicopter
    Society, Vol. 17, No. 1, January 1972, pp. 41-48.

7.  Landgrebe, A. J., "The Wake Geometry of a Hovering
    Helicopter Rotor and Its Influence on Rotor Performance",
    28th Annual National Forum American Helicopter Society,
    Preprint No. 620, May 1972.

8.  Curtiss, H. C. Jr. and Shupe, N. K., "A Stability and
    Control Theory for Hingeless Rotors", 27th Annual
    National Forum of the American Helicopter Society, Pre-
    print No. 541, May 1971.

9.  Ormiston, R. A., and Peters, D. C., "Hingeless Rotor
    Response with Non-uniform Inflow and Elastic Blade
    Bending . . . Theory and Experiment", AIAA 10th Aerospace
    Science Meeting, AIAA Paper No. 72-65, January 1972.

10. Kuczynski, W. A., Sharpe, D. L., and Sissingh, G. J.,
    "Hingeless Rotor-Experimental Frequency Response and
    Dynamic Characteristics with Hub Moment Feedback Controls",
    28th Annual National Forum of American Helicopter Society,
    Preprint No. 612, May 1972.

11. Yin, S. K., and Hohenemser, K. H., "The Method of Multi-
    blade Coordinates in the Linear Analysis of Lifting Rotor
    Dynamic Stability and Gust Response", 27th Annual
    National Forum of the American Helicopter Society, Pre-
    print No. 512, May 1971.

## Figure Captions

Fig. 1    Blade Flapping Angle in Progressing and Regressing Mode

Fig. 2    Schematic of Rotor Hub and Pitch Control

Fig. 3    Schematic Side View of Rotor Model in Wind Tunnel Section, Rotor in Tunnel Center

Fig. 4    Blade Flap Bending Moment per inch of Tip Deflection

Fig. 5    First Blade Flap Bending Mode

Fig. 6    Coning Angle vs. Collective Pitch Angle for $\mu = 0$

Fig. 7    Rotor Tilting Amplitudes per Unit Cyclic Pitch Amplitude, $\mu = 0$, $\Theta_o = 5°$

Fig. 8    Phase Angles, $\mu = 0$, $\Theta_o = 5°$

Fig. 9    Rotor Tilting Amplitudes per Unit Cyclic Pitch Amplitude, $\mu = .2$, $\Theta_o = 5°$

Fig. 10    Phase Angles, $\mu = .2$, $\Theta_o = 5°$

Fig. 11    Rotor Tilting Amplitudes per Unit Cyclic Pitch Amplitude, $\mu = .4$, $\Theta_o = 5°$

Fig. 12    Phase Angles, $\mu = .4$, $\Theta_o = 5°$

Fig. 13    Rotor Tilting Amplitude per Unit Cyclic Pitch Amplitude, $\mu = 0$, $\Theta_o = 2°$

Fig. 1



a.
progressing

$$\frac{2\pi}{1-\omega}$$

b.
regressing
$P > 1 + \omega$

$$\frac{2\pi}{1+\omega}$$

c.
regressing
$P < 1 + \omega$

$$\frac{2\pi}{1+\omega}$$

$$2\pi$$
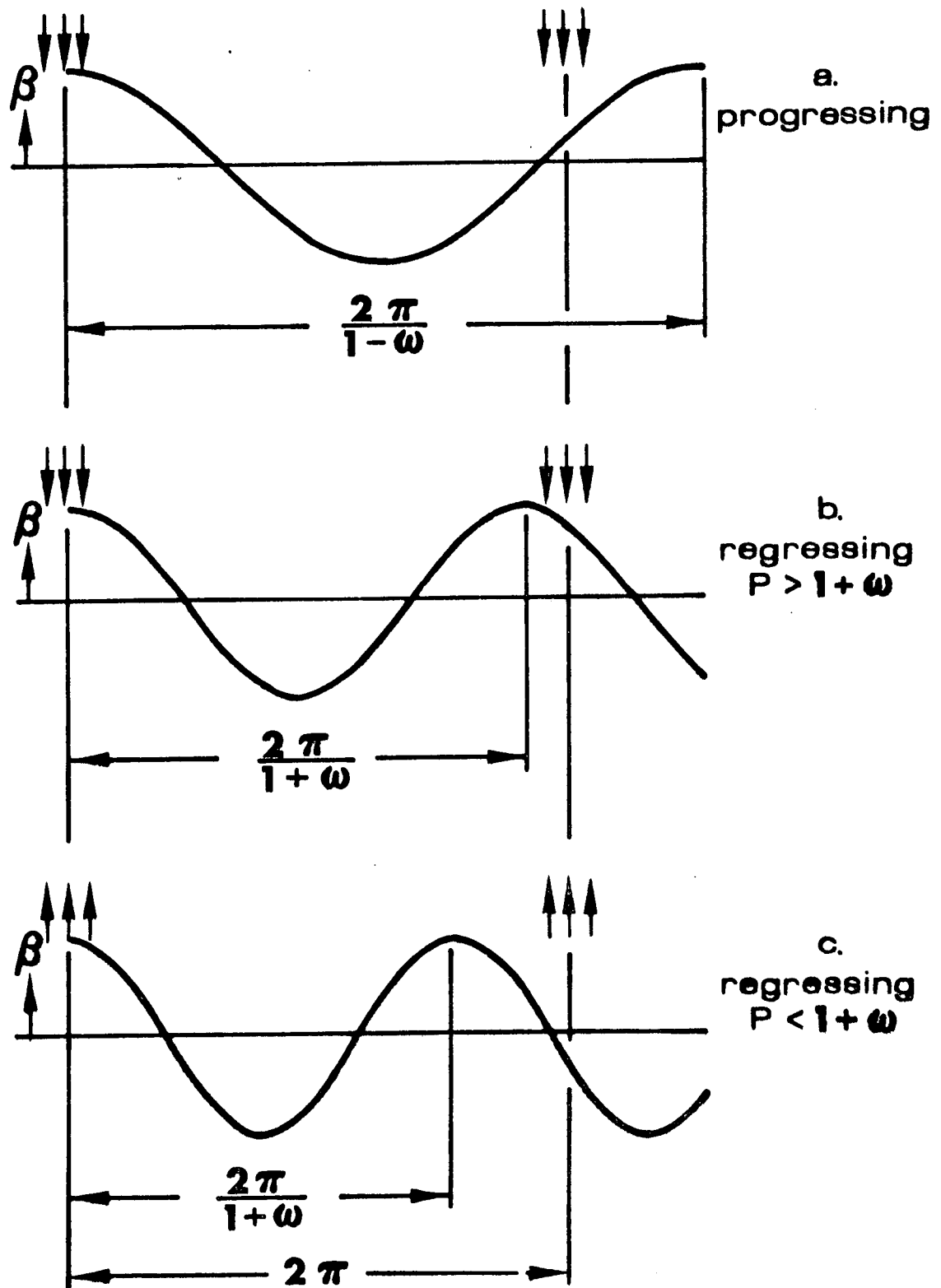
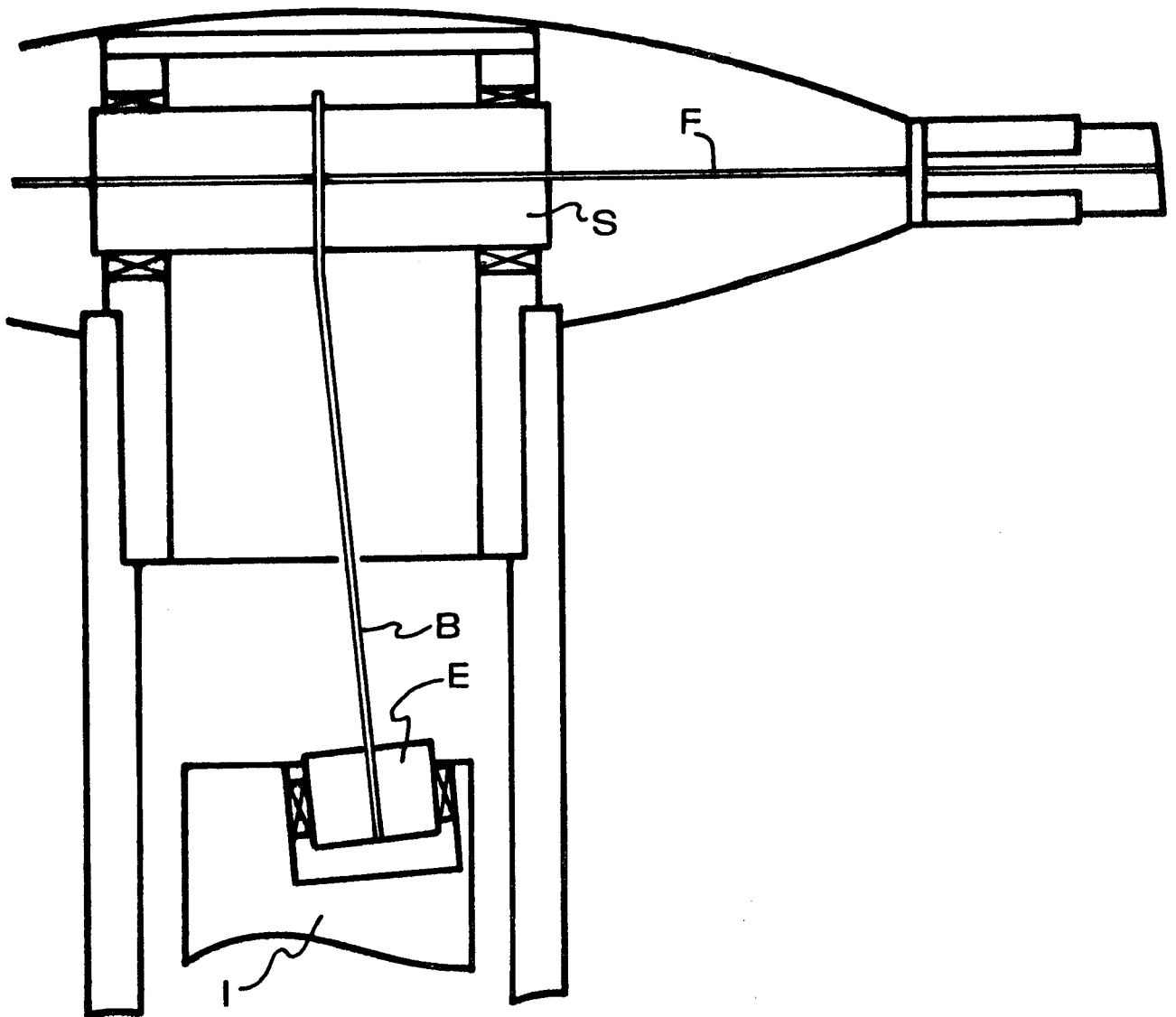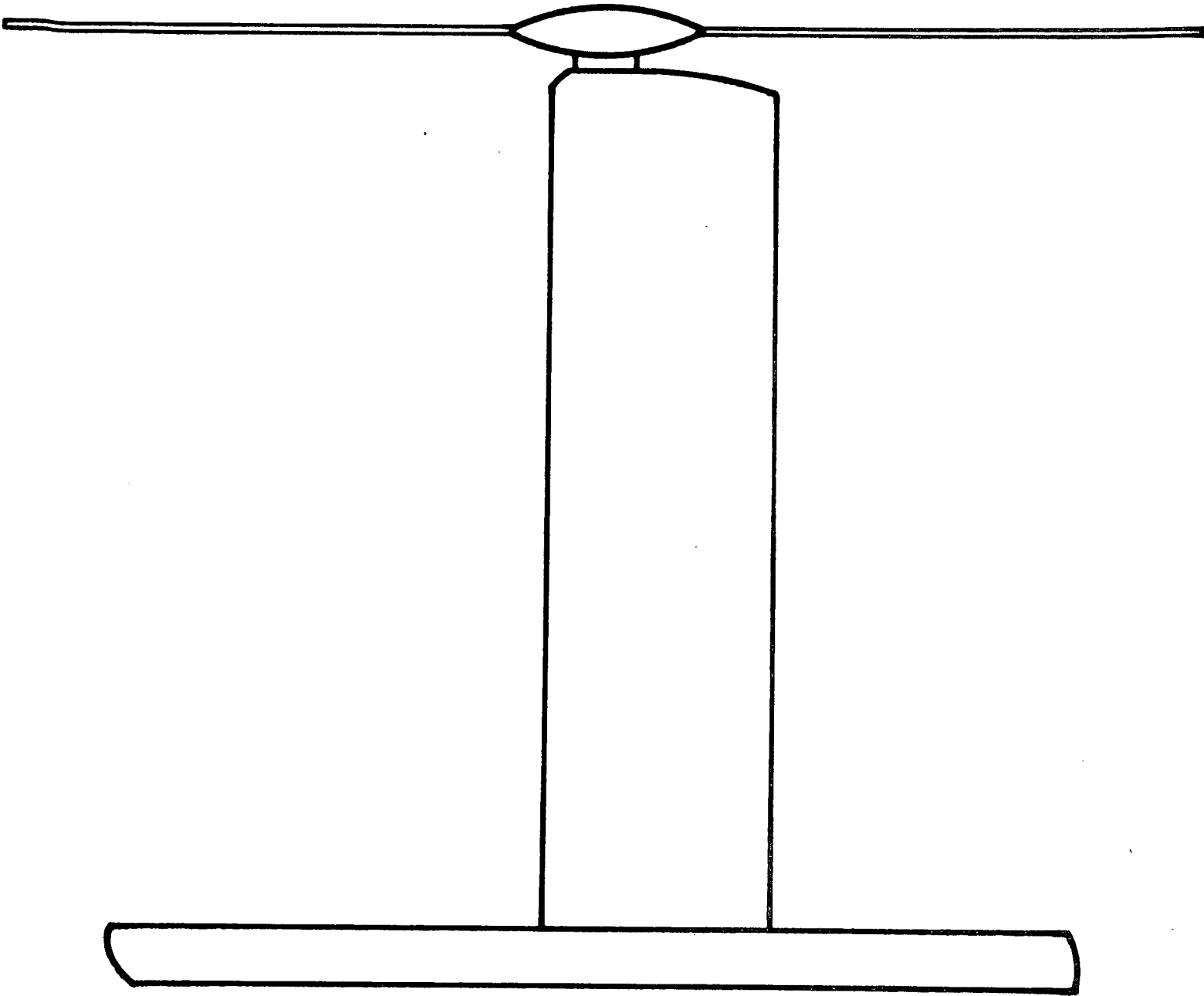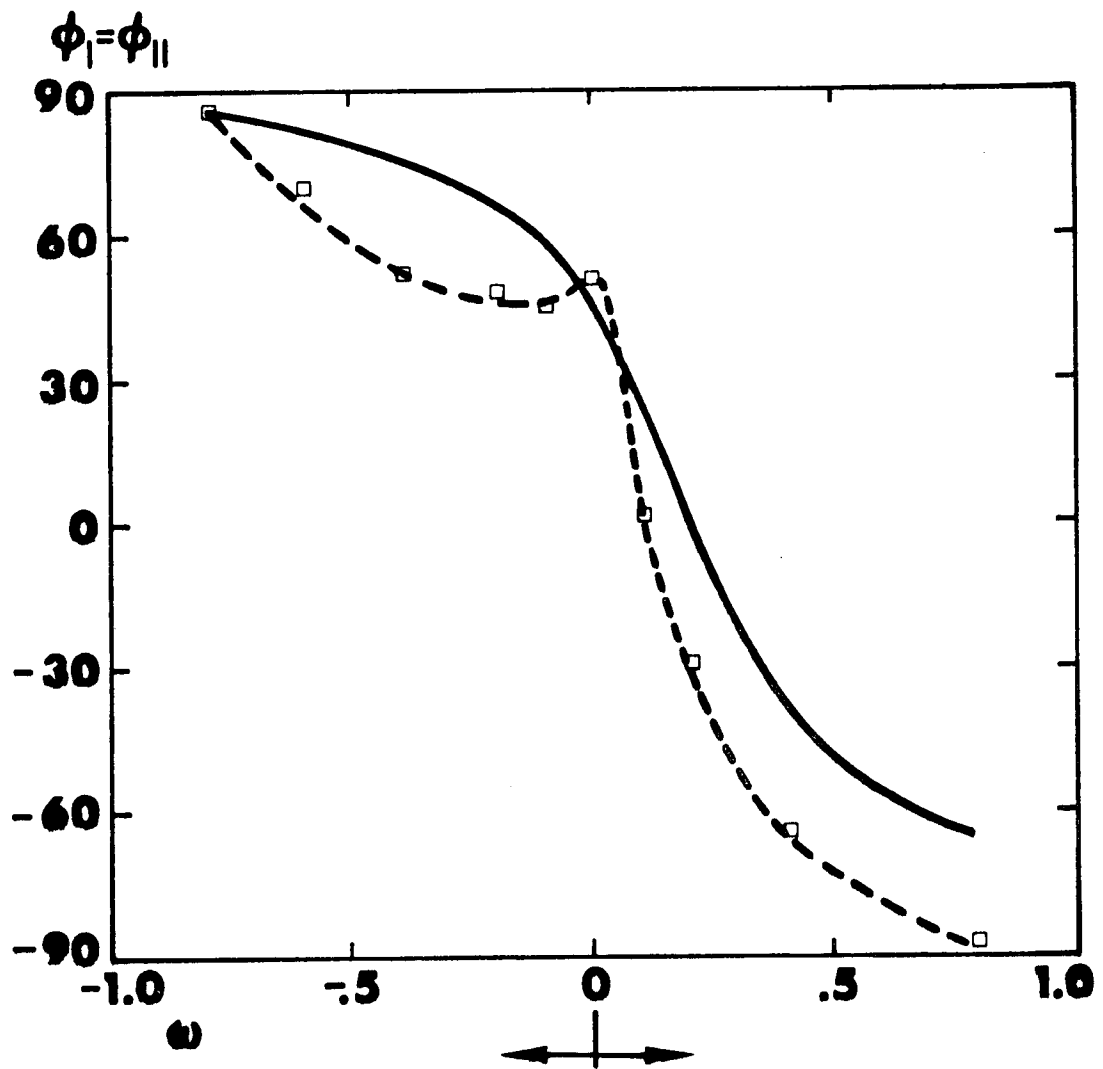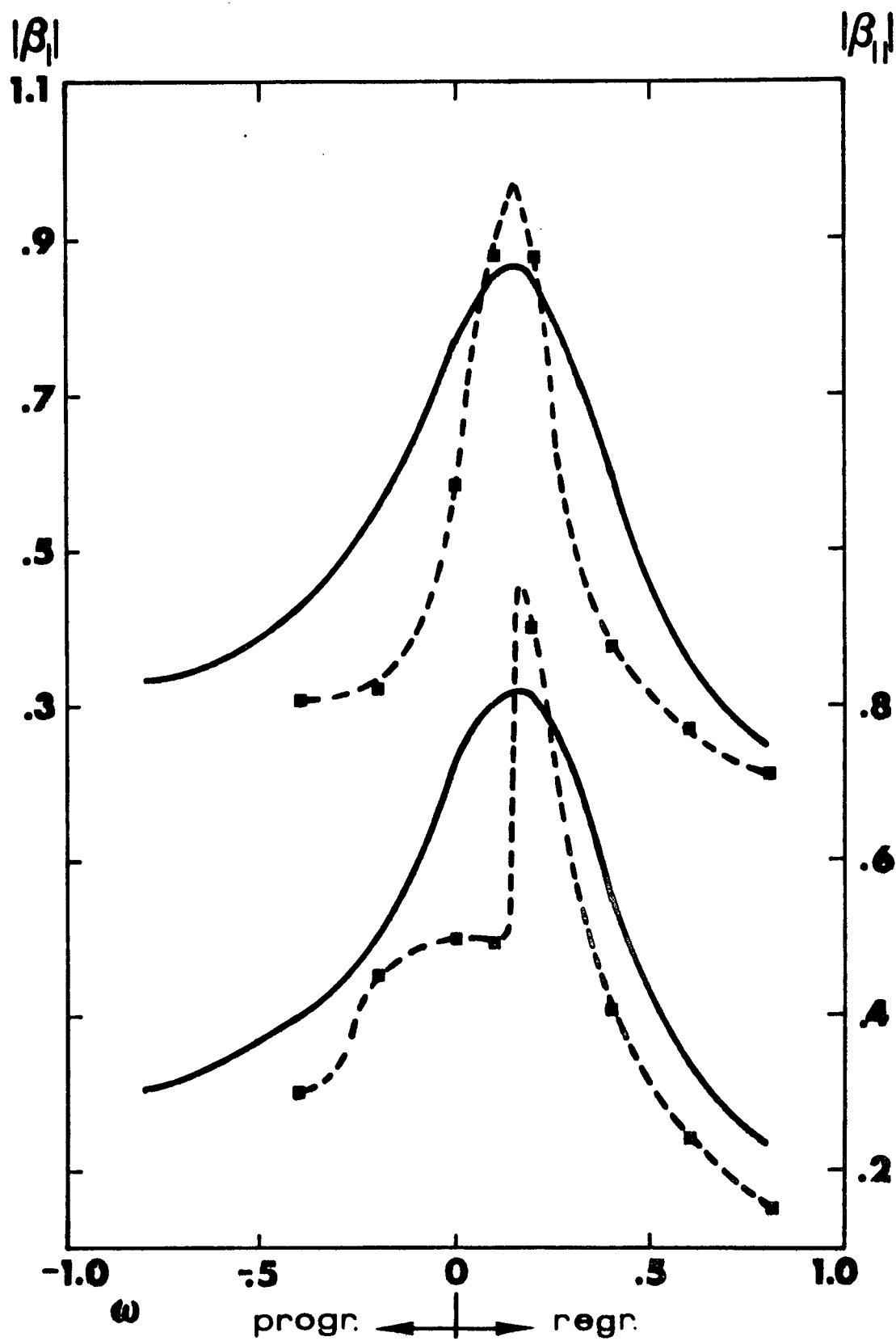Fig. 2

Fig. 3

Fig. 4
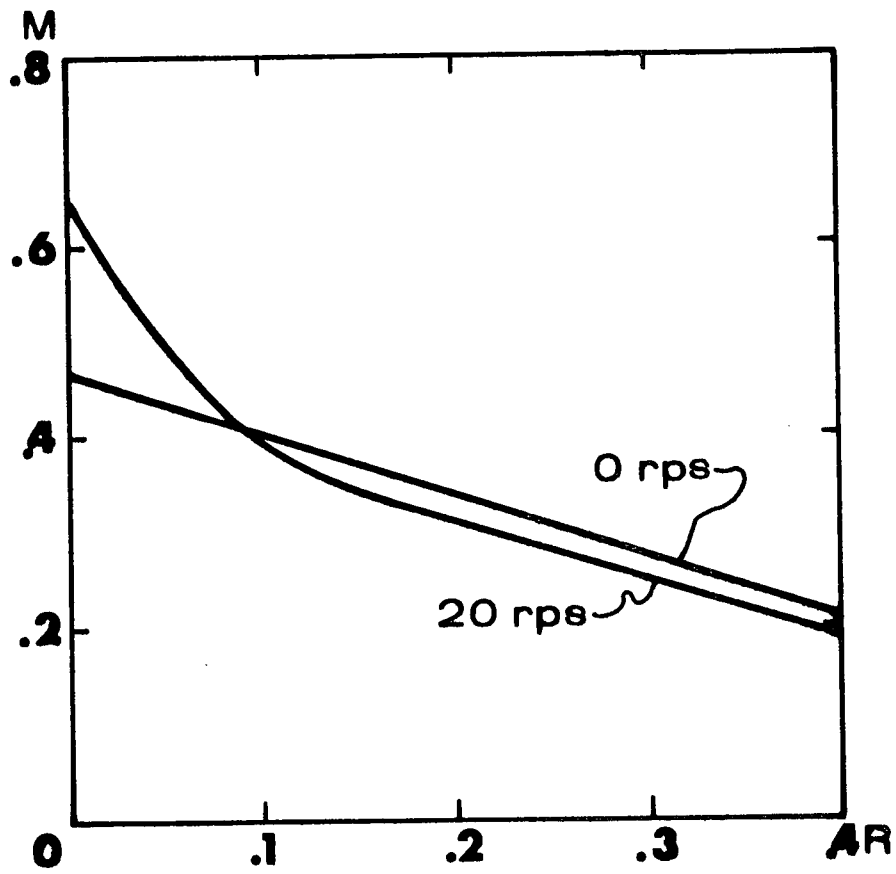
Fig. 5
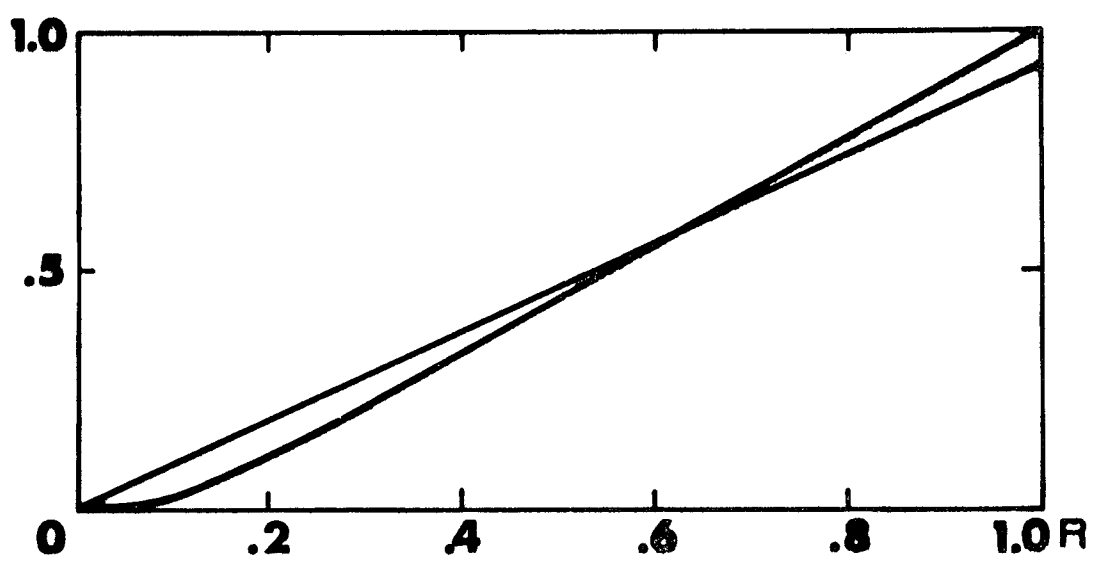
Fig. 6
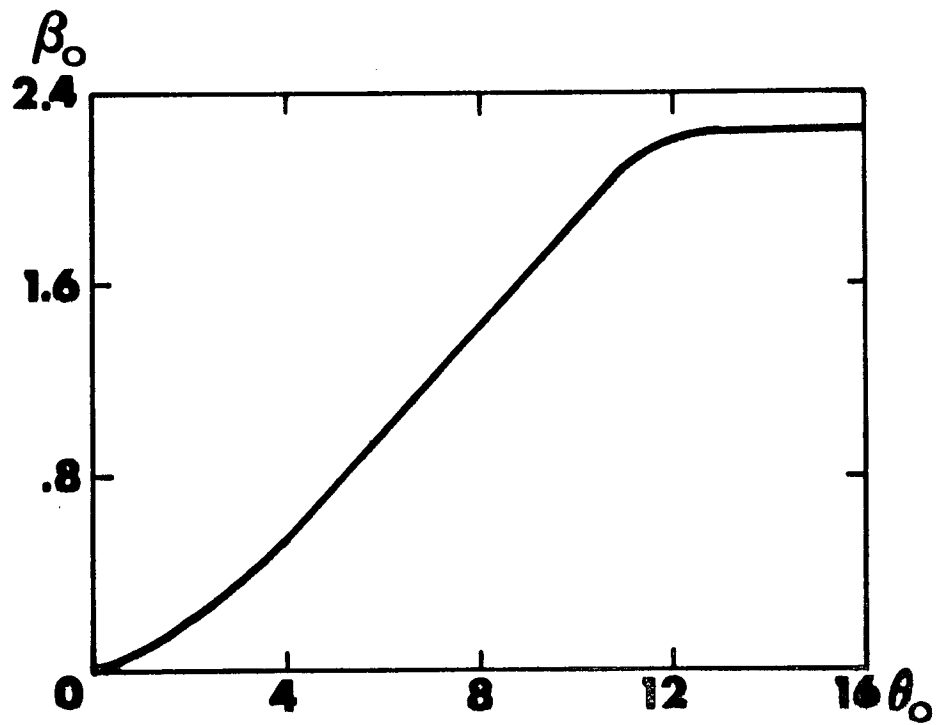
Fig. 7
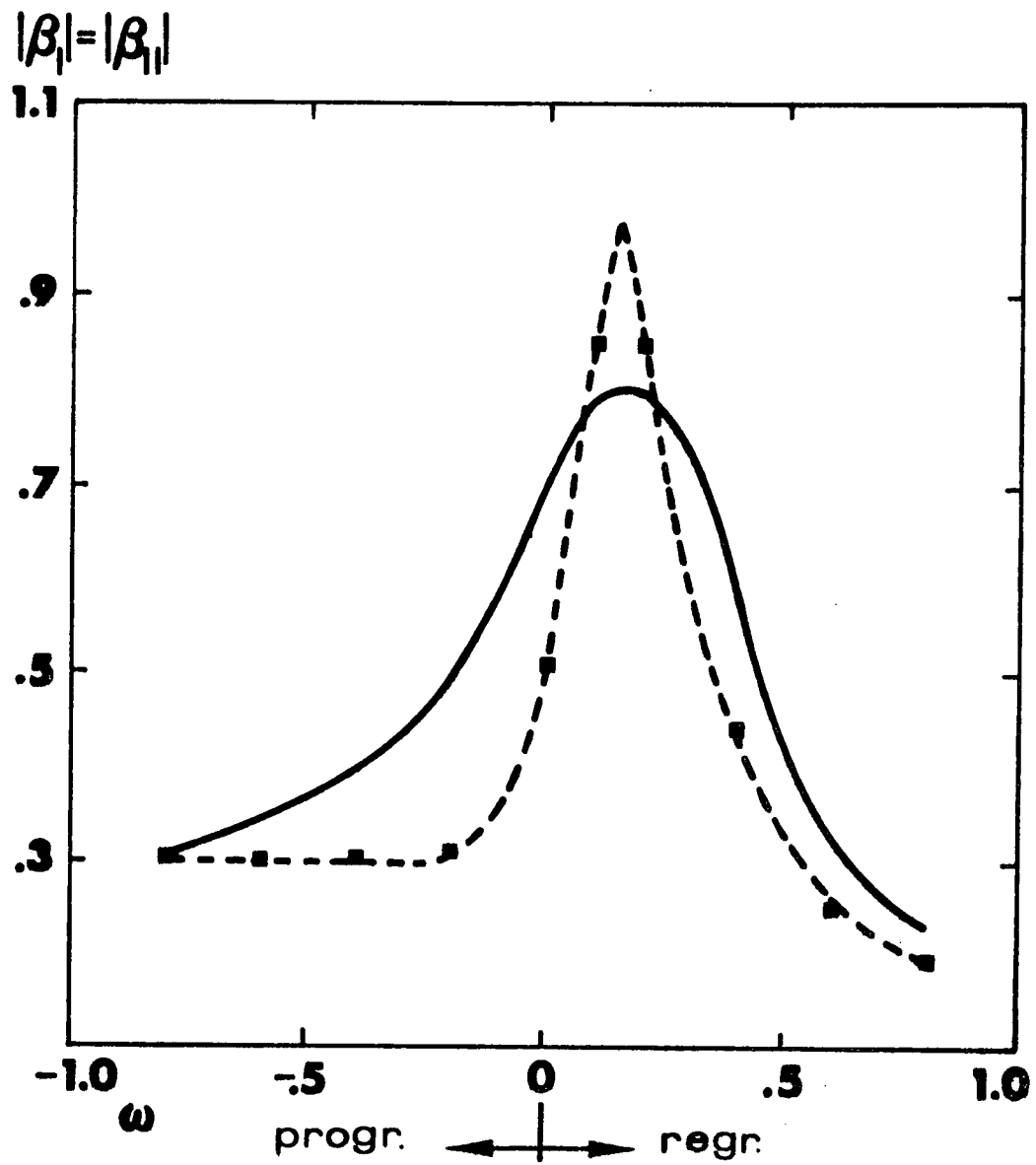
Fig. 8

Fig. 9
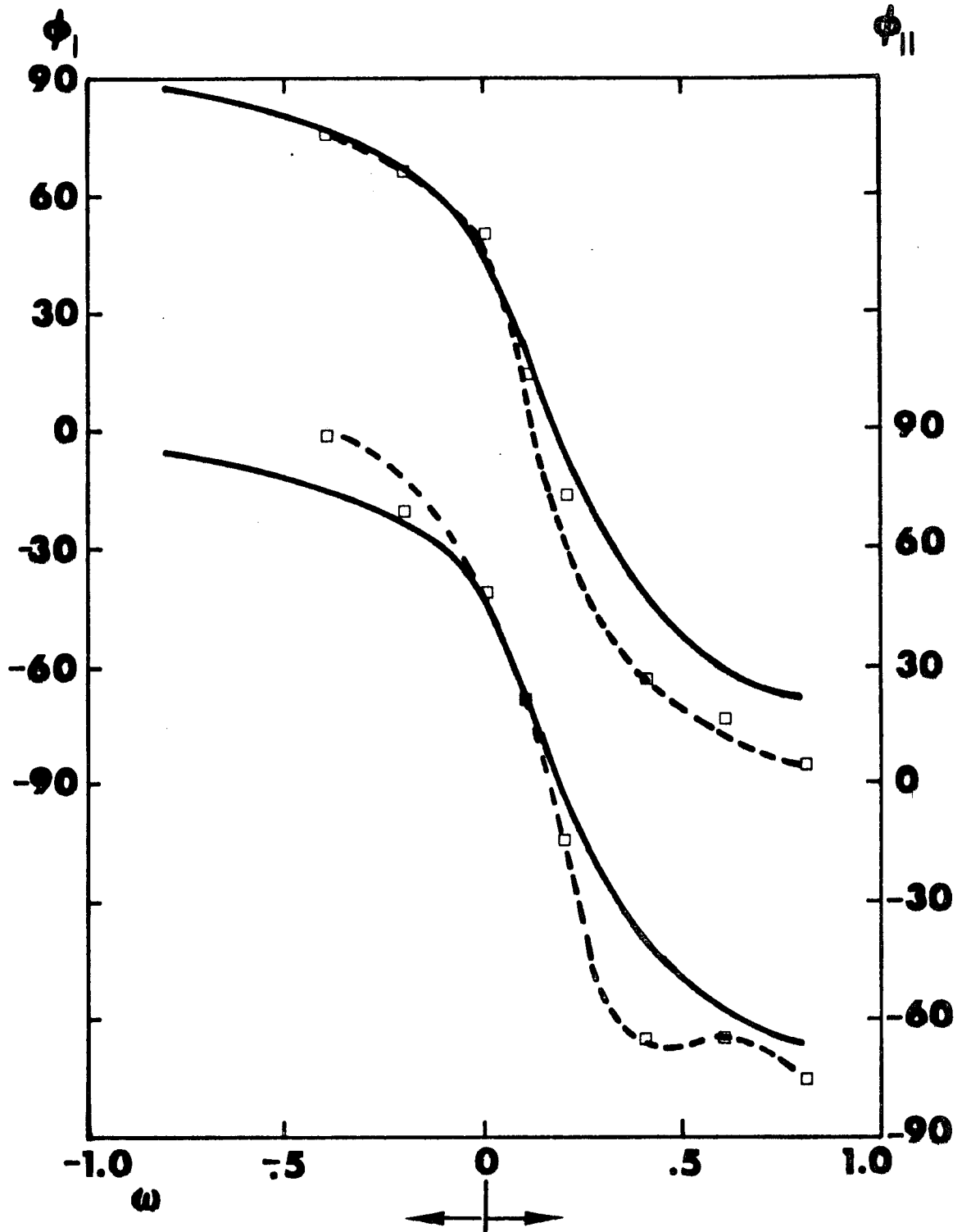
Fig. 10
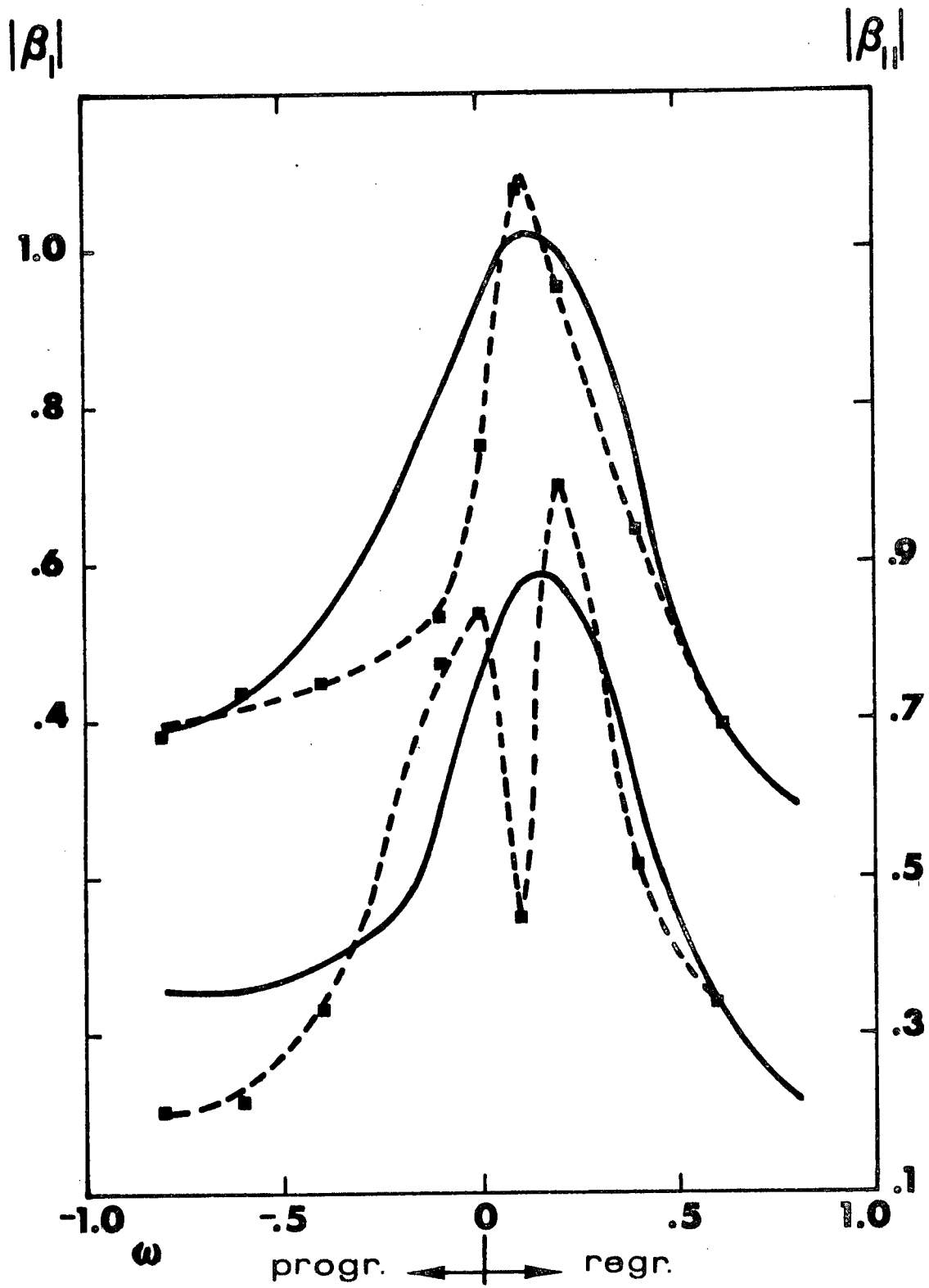
Fig. 11
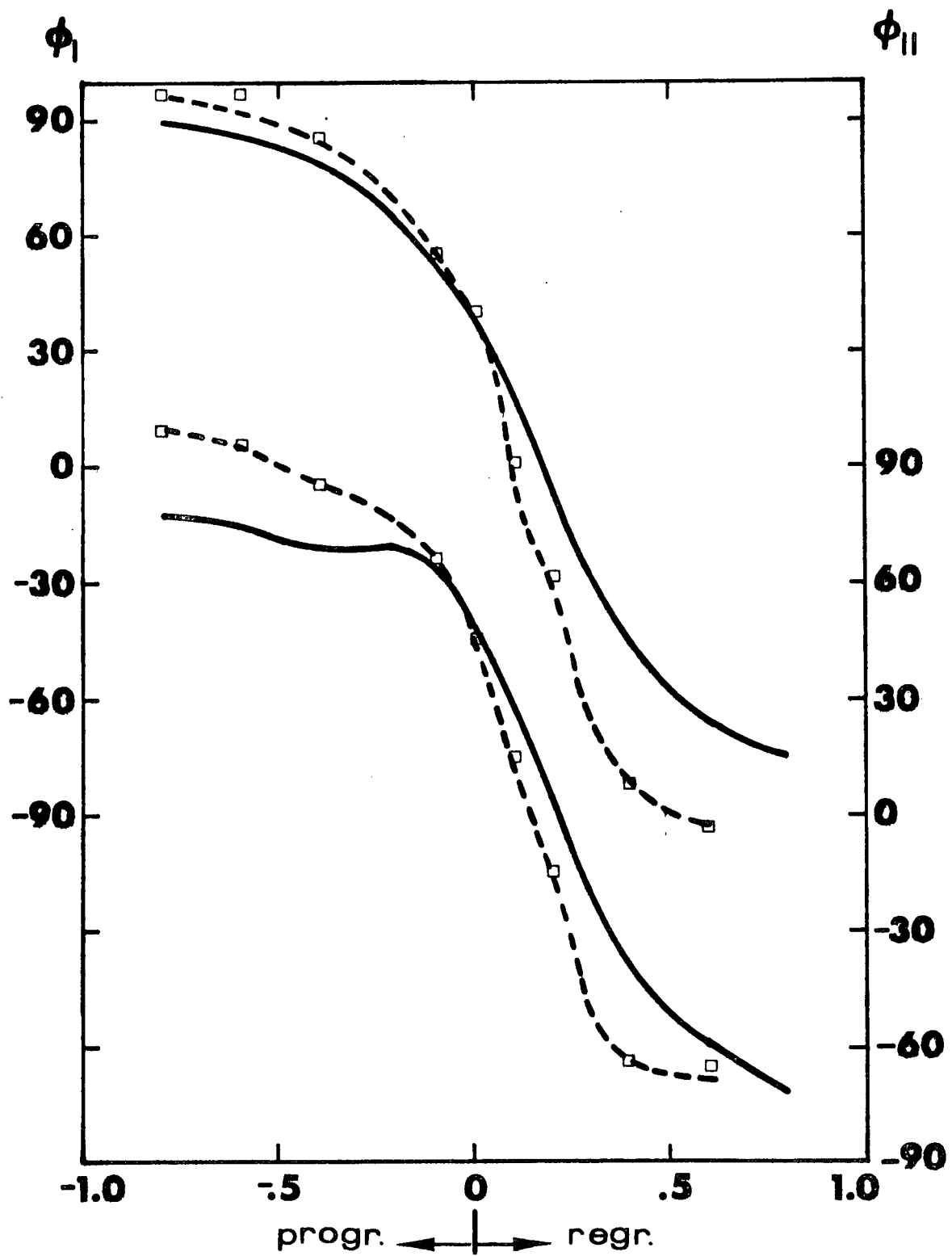
Fig. 12
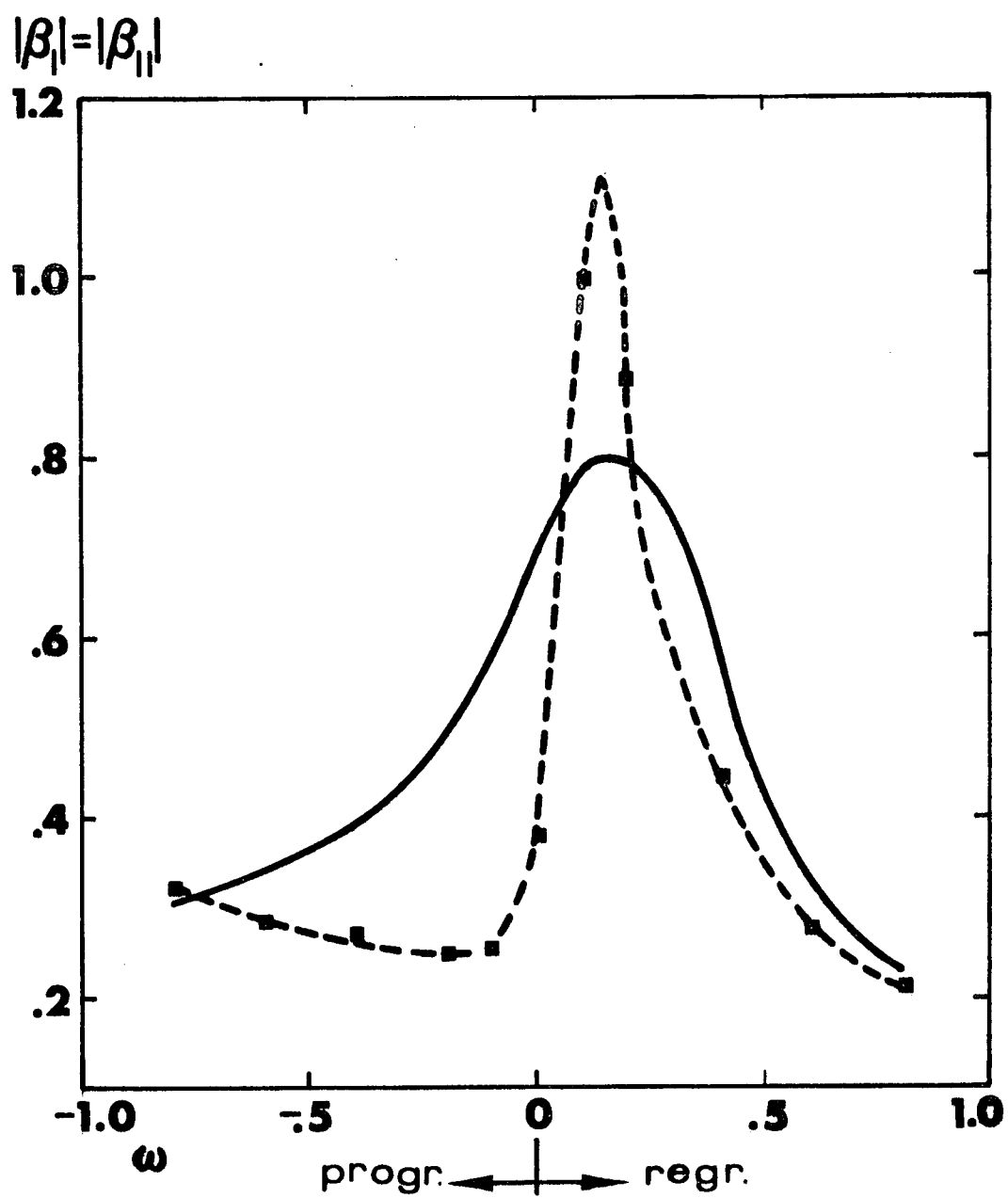
Fig. 13

## Appendix A

### Computation of Undamped Blade Modes

#### Nomenclature

| | |
|---|---|
| $\Omega$ | rotor angular speed ($1/\Omega$ is the time unit) |
| $R$ | rotor radius (length unit) |
| $m_o$ | mass per unit length of blade root |
| $m_o R$ | mass unit |
| $m_o R^2 \Omega^2$ | force unit |
| $T_i m_o R^2 \Omega^2$ | centrifugal force in ith massless segment |
| $m_i m_o R$ | point mass between massless segments |
| $x_i R$ | distance of $m_i$ from rotor center |
| $\Delta T_i m_o R^2 \Omega^2$ | centrifugal force of ith point mass |
| $y_i R$ | up deflection of $m_i$ |
| $\psi_i$ | slope of deflection curve at $m_i$ |
| $l_i R$ | length of ith segment |
| $(EI_i) q\, m_o R^4 \Omega^2$ | bending stiffness of ith segment assumed constant |
| $EI_o$ | bending stiffness at blade root |
| $M_i m_o R^3 \Omega^2$ | bending moment at $m_i$ |
| $S_i m_o R^2 \Omega^2$ | shear force to the left of $m_i$ |
| $\omega \Omega$ | frequency of harmonic oscillation of blade |
| $q = EI_o / m_o R^4 \Omega^2$ | non-dimensional bending stiffness of blade root |
| $X_i$ | state vector at $m_i$ with the 4 components $y_i,\ \psi_i,\ M_i,\ S_i$ |
| $\phi_i$ | state transition matrix relating $X_i$ to $X_{i+1}$ |

$X_i^{(1)}$        state vector for free end conditions
$y_1 = 1$, $\psi_1 = M_1 = S_1 = 0$

$X_i^{(2)}$        state vector for free end conditions
$\psi_1 = 1$, $y_1 = M_1 = S_1 = 0$

Fig. A-1 shows a massless blade segment with point mass at the left end in its maximum up position during a harmonic oscillation with circular frequency $\omega$. The centrifugal force $T_i$ along the element is assumed to be constant and to change only at the mass:

$$T_i = T_{i-1} + \Delta T_i \tag{A-1}$$

where

$$\Delta T_i = m_i x_i \tag{A-2}$$

Since the blade tip is to the left

$$T_i = \sum_{k=1}^{i} \Delta T_k \tag{A-3}$$

We resolve the centrifugal force $T_i$ at the left end of the segment - but to the right of the mass - into a component along the deflected blade axis and a component $\psi_i T_i$ perpendicular to it. Deflection and slope at i+1 are

$$y_{i+1} = y_i + \psi_i \ell_i + M_i \ell_i^2/2qEI_i + (S_i + y_i m_i \omega^2 + \psi_i T_i)\ell_i^3/6qEI_i \tag{A-4}$$

$$\psi_{i+1} = \psi_i + M_i \ell_i/qEI_i + (S_i + y_i m_i \omega^2 + \psi_i T_i)\,\ell_i^2/2qEI_i \tag{A-5}$$

The moment equilibrium about the right end of the segment yields

$$M_{i+1} = M_i + (S_i + y_i m_i \omega^2 + \psi_i T_i)\,\ell_i \tag{A-6}$$

The vertical force equilibrium yields

$$S_{i+1} = S_i + m_i y_i \omega^2 \tag{A-7}$$

Using the state vector

$$X_i = \begin{Bmatrix} Y_i \\ \psi_i \\ M_i \\ S_i \end{Bmatrix} \tag{A-8}$$

the transition from $X_i$ to $X_{i+1}$ is according to Eqs. (A-4) to (A-7)

$$X_{i+1} = \phi_i X_i \tag{A-9}$$

with the state transition matrix

$$\phi_i = \begin{bmatrix} 1 + m_i \omega^2 \ell_i^3/6qEI_i & \ell_i + T_i \ell_i^3/6qEI_i & \ell_i^2/2qEI_i & \ell_i^3/6qEI_i \\ m_i \omega^2 \ell_i^2/2qEI_i & 1 + T_i \ell_i^2/2qEI_i & \ell_i/qEI_i & \ell_i^2/2qEI_i \\ m_i \omega^2 \ell_i & T_i \ell_i & 1 & \ell_i \\ m_i \omega^2 & 0 & 0 & 1 \end{bmatrix} \tag{A-10}$$

Combining the n fields:

$$X_{n+1} = \phi_n \phi_{n-1} \cdots \phi_1 X_1 \tag{A-11}$$

$X_1$ at the tip of the blade has the unknowns $y_1, \psi_1$, while $M_1 = S_1 = 0$. We compute $X_{n+1}^{(1)}$ and $X_{n+1}^{(2)}$ for free end conditions $X_1^{(1)} = \begin{Bmatrix} 1 \\ 0 \\ 0 \\ 0 \end{Bmatrix}$, and $X_1^{(2)} = \begin{Bmatrix} 0 \\ 1 \\ 0 \\ 0 \end{Bmatrix}$.

$$Y_1 \, Y_{n+1}^{(1)} + \psi_1 \, Y_{n+1}^{(2)} = 0$$

$$\tag{A-12}$$

$$Y_1 \, \psi_{n+1}^{(1)} + \psi_1 \, \psi_{n+1}^{(2)} = 0$$

The frequency equation is

$$\begin{vmatrix} Y_{n+1}^{(1)} & Y_{n+1}^{(2)} \\ \\ \psi_{n+1}^{(1)} & \psi_{n+1}^{(2)} \end{vmatrix} = 0 \tag{A-13}$$

The only unknown in Eq. (A-13) is $\omega$. By iterating $\omega$ until Eq. (A-13) is satisfied, one obtains the natural frequencies. For each natural frequency one obtains for $y = 1$ from the first of Eqs. (A-12)

$$\psi_1 = - \, Y_{n+1}^{(1)} \, / \, Y_{n+1}^{(2)} \tag{A-14}$$

so that now $X_i$ can be computed for each i beginning with the known state vector

$$X_1 = \begin{Bmatrix} 1 \\ \psi_1 \\ 0 \\ 0 \end{Bmatrix} \tag{A-15}$$

For regions of large curvature small segments $\ell_i$ are required, while for regions with little curvature the lengths $\ell_i$ can be larger. Using 20 segments the computation of two natural frequencies with associated modes takes on the IBM 360-50 computer about 10 CPU seconds. For given $m_i$ and $EI_i$ the natural frequencies depend only on q. For small q we have $\omega_1 = 1.0$, for large q we have

$$\omega_1 / q^{1/2} = \alpha \tag{A-16}$$

whereby

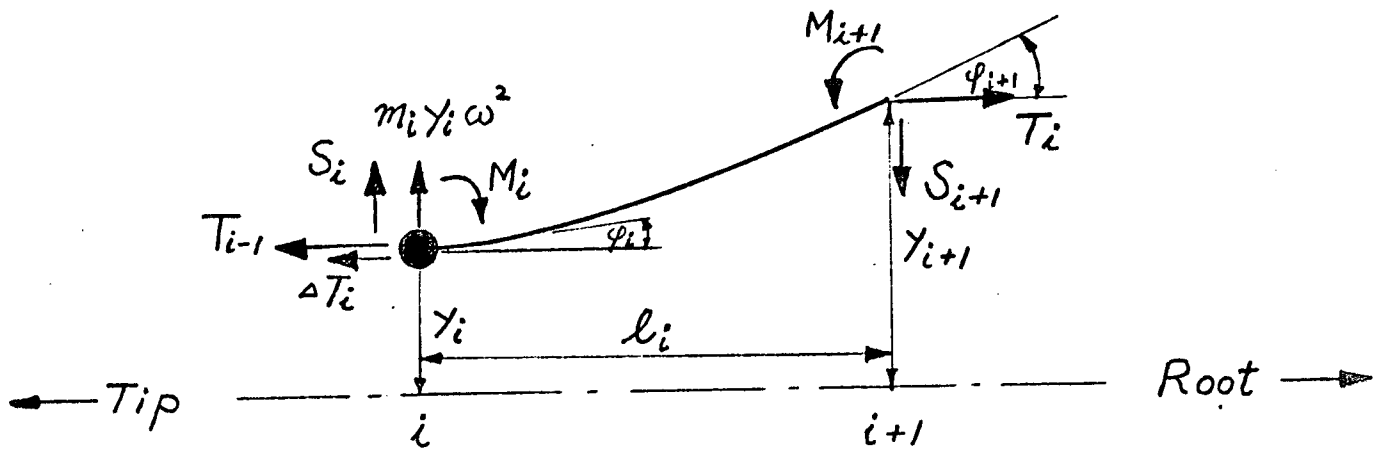$$\omega_1 \Omega = \frac{\alpha}{R^2} \left( \frac{EI_o}{m_o} \right)^{1/2}$$

(A-17)



Fig. A-1

# Appendix B

## Model Development

### 1. Rotor Development

### 1.1 Blade Development

All tests so far have been conducted with the balsa blades. Tracking the blades at various advance ratios revealed that one of the blades possessed some camber. At low advance ratios ($\mu = 0, .5$), the tracking errors due to the difference in camber of the two blades was small and could be neglected. At higher advance ratios the error was too large to be ignored and could only be corrected by adjusting the collective pitch setting of one of the blades.

Four new fiberglass coated styrofoam blades have been ordered from the Princeton University model shop. They are made from a mold and should be identical. The future high advance ratio tests will be made with these blades.

### 1.2 Blade-Hub Attachment Development

The original blade-hub was designed with flapping hinges which are stiff in torsion and soft with respect to axial load and with respect to in-plane moments. Most of the axial load is carried by the center strap which also carries most of the in-plane moments. The new blade-hub attachment (Fig. B - 1) is a simple strap .015" thick (3 times as thick as the previous strap) which carries all loads. At a given rotor speed, the new attachment has a higher P-value than

the hinged rotor.

## 1.3  Hinged Rotor Results

Fig. B-2 shows for zero wind velocity the absolute mag-
nitude of the ratio flapping amplitude over feathering ampli-
tude vs. non-dimensional excitation frequency in the rotating
frame of reference using ±3° feathering excitation for three
values of the collective pitch, 0, 3°, and 6°.  Also shown
in the figure is the calculated absolute magnitude of the
amplitude ratio, using uniform inflow and the measured
natural flapping frequency at zero rpm, which is 5 cps.
The rotorspeed was 44 cps and the non-dimensional flapping
frequency square at this speed is obtained from the hinge-
offset and the non-rotating natural frequency as

$$P^2 = 1 + 1.5 \ \frac{\ell/R}{1-\ell/R} + (5/44)^2 = 1.0 + .143 + .0113 = 1.16$$

It is seen that the flexure contributes very little to the
stiffness, so that the "P" value is over a wide rotorspeed
range approximately constant.  The Lock inertia number,
defined with the blade flapping mode shape $\xi$ as

$$\gamma = a\rho cR/\int_0^1 \xi^2 md \quad \text{(m is the blade mass per unit length)}$$

is 4.5, so that the differential equation of blade flapping
motion becomes

$$\ddot{\beta} + .56\dot{\beta} + 1.16\beta = .56\theta e^{i\omega t}$$

where $\theta$ is the feathering amplitude.

From Fig. B-2 it is seen that the theoretical amplitude ratio is at the resonance point smaller than the measured amplitude ratio, while above and below resonance the measured amplitude ratios are substantially smaller. Fig. B-3 shows the amplitude ratios at zero collective pitch setting for 3 values of feathering amplitude: ±1.5°, ±3°, ±4.5°. The trend is the same. Note that the largest feathering amplitude of ±4.5° produces at resonance a flapping amplitude ratio somewhat larger than for ±3° and ±1.5°. Also note that at $\omega = 1.0$ the measured amplitude ratio is in some cases substantially smaller than the predicted one, which means that the control power for a rotor with off-set hinges can be substantially less than predicted by the usual analysis.

Since these results, if correct, would have rather important consequences for rotors with large hinge off-sets or for hingeless rotors, it was believed necessary to first check the mechanical properties of the model carefully before proceeding with the wind-on tests, in order to make sure that the deviations of the test results from the theoretical results indicated in Figs. B-2 & B-3 are caused by aerodynamic rather than mechanical effects.

First the response tests at zero wind were repeated with 4 different rotor rotational frequencies: 17, 22, 32, 44 cps. As mentioned before, the "P" value is approximately independent of rotor speed in this region and was throughout close to P = 1.08. The test covered three feathering amplitudes

±1.5°, ±3°, ±4.5° and two collective pitches, 0° and 6°.
The amplitude ratios vs. excitation frequency showed for all
these tests basically the same characteristics presented in
Figs. B-2 & B-3 for 44 cps rotational frequency, though
with some minor variations.

The blades have some mechanical damping in the flapping
hinges which was studied rather carefully in a rig in which
the blade could be loaded by a tension wire of .010" diameter,
attached to the blade tip guided over a pulley and held under
tension by weights. The tension was adjusted to give the
blade flapping frequencies corresponding to those at the 4
rotation frequencies of 17, 22, 32 and 44 cps. The free
blade oscillations following an impulse were recorded and
evaluated with respect to the type and amount of damping
present. Since the pulley performed small oscillations,
the measured damping includes that of the pulley and is con-
servative. It was found that the decay characteristics of
the blade flapping oscillation could be explained by a com-
bination of viscous and Coulomb damping.

The viscous damping was found to be in the order of $C = .0040$ inch pounds per radians per second. The damping ratio
from mechanical viscous damping is then

| cps | 17 | 22 | 32 | 44 |
|-----|------|------|------|------|
| $\zeta_m$ | .032 | .025 | .017 | .013 |

This compares with a predicted aerodynamic damping ratio $\zeta_a$
from $2\zeta_a P = \gamma/8$, $\zeta_a = .26$.

The mechanical viscous damping is, therefore 5 to 12% of the predicted aerodynamic damping, depending on the rotor-speed.

Of more concern is the Coulomb damping, which became important at small amplitudes and at low frequencies, since the equivalent linear damping is

$$C = 4M_F/\pi\omega x$$

While the effect of Coulomb damping was definitely small in the region of amplitudes shown in Figures 2 and 3 with 44 cps rotational frequency and $\pm 1.5°$ to $\pm 4.5°$ feathering excitation, the Coulomb damping does become more significant at smaller excitation amplitude.

In summary it can be said, that for the cases presented in Figs. B-2 & B-3 the predicted response curve in the vicinity of the resonance needs only small corrections from mechanical damping. The low amplitude low rotor speed cases, however, require a not negligible correction from mechanical damping. Because of the non-linearity of part of the damping the application of corrections would become quite cumbersome and the simplicity of the linear aerodynamic theory would be sacrificed. It was, therefore decided to modify the model before proceeding with the testing at non zero wind.

## 1.4   The New Rotor Configuration

The new rotor configuration was instrumented for flapping and torsion response measurements. By exciting the rotor

near the blade root with a magnetic pickup and using the
flapping and torsion instrumentation on the blade-hub
flexures, the first, second and third natural flapping
frequencies were found to be 11.6 cps, 151 cps, and 385 cps
respectively at 0 rps, and the first torsional frequency
was found to be 180 cps at 0 rps. The first torsional
frequency at 20.3 rps was found to be 184 cps using the
experimental set-up used in making the damping measurements
(which cannot simulate the so-called tennis racket effect,
which would slightly increase the torsional frequencies).
The blade mass distribution is shown in Fig. B-4. A finite
element analysis using 20 elements ( shown on the figure)
used the experimentally determined first and second natural
flapping frequencies to construct the unknown blade stiff-
ness distribution (Fig.B-4). The analysis was then used to
determine the mode shapes and the flap bending moments both
rotating and non-rotating. Fig. B-5 shows the first and
second flap bending frequencies versus rotor rps. The rps
at which tests are being conducted are marked.

2.   Rotor Control System Development

The cyclic pitch excitation system is shown in Figure
2 of the main report. It consists of an oscillating shaft
which transmits the pitch input from the eccentric flexure
to the blade-hub attachment. The two halves of the oscil-
lating shaft have 12 degrees of rotational freedom so that

they can be adjusted with respect to each other and with
respect to the eccentric flexure. Tracking of the blades
and collective pitch inputs are achieved by proper adjust-
ment of these elements with respect to each other.

The eccentric flexure translates the circular motion
of the eccentric into the pitching motion of the oscillating
shaft. Three eccentrics with different amounts of eccentri-
city are available. They have the capability of transmitting
±1.5, ±3.0, or ±4.5 degrees pitching angle to the blade.
Each eccentric is fitted with an Oilyte Bearing.

The original drive system consisted of two motors one
of which drove the rotor shaft and one of which drove the
pitch control shaft (which is inside the rotor shaft) which
rotates the eccentric. The sum of the rotational velocities
of the two motors determines the cyclic pitch frequency
excitation and phasing. The two motors were operated
through separate control circuitry. Though at zero advance
ratio 100-200 cycles could be held with only ±2° phase
error, when wind-on testing began, it quickly became
obvious that obtaining the proper phasing with the separate
motor control systems was too difficult to be practical.
Therefore, a gear drive was installed between the rotor and
pitch shaft and the whole system is now driven by the rotor
shaft motor. The system is shown in Fig. B-6.

The gear drive consists of a permanent gear on the rotor
shaft which drives a primary gear on a removable shaft.

There is a 5 to 1 speed step-down between the rotor shaft
gear and the primary gear on the removable shaft. There
are 4 sets of gears, which have the same center to center
distances as the center to center distance between the rotor
gear and primary removable shaft gear, with gear ratios of
1/1, 2/1, 3/1 and 4/1. By using different sets of gears
between the removable pitch control shaft, and by inter-
changing the gears in a set between the removable shaft and
the pitch control shaft, pitching frequency excitations of
.2P, .4P, .6P, .8P, .9P, .925P, and .95P can be achieved.
The primary gear on the removable shaft can be moved so
that a reversing set of gears can be put between the rotor
gear and the primary removable shaft gear. This allows
pitching frequency excitations of 1.05P, 1.075P, 1.10P,
1.20P, 1.40P, 1.60P and 1.80P. Phasing is achieved by
adjusting the positioning between the rotor and pitch con-
trol shaft before tightening the final set screw at each
testing frequency. It takes from 2 to 3 hours to go through
the series of pitch frequency excitations, which is not an
unreasonable amount of time to spend to get one wind-on
test set performed.

3. Measuring Equipment Development

In addition to the measuring equipment listed in
Phase V-C Report there is a torsion strain gauge on one of
the blade flexures.

Figure I   Rotor Configuration

Figure B-2



± 3 degree Excitation

Response
Excitation

Linear Equation of Motion:
$\ddot{\theta} + .56\dot{\theta} + .03\ddot{\theta} + 1.16\,\theta = .56\theta e^{i\omega t}$
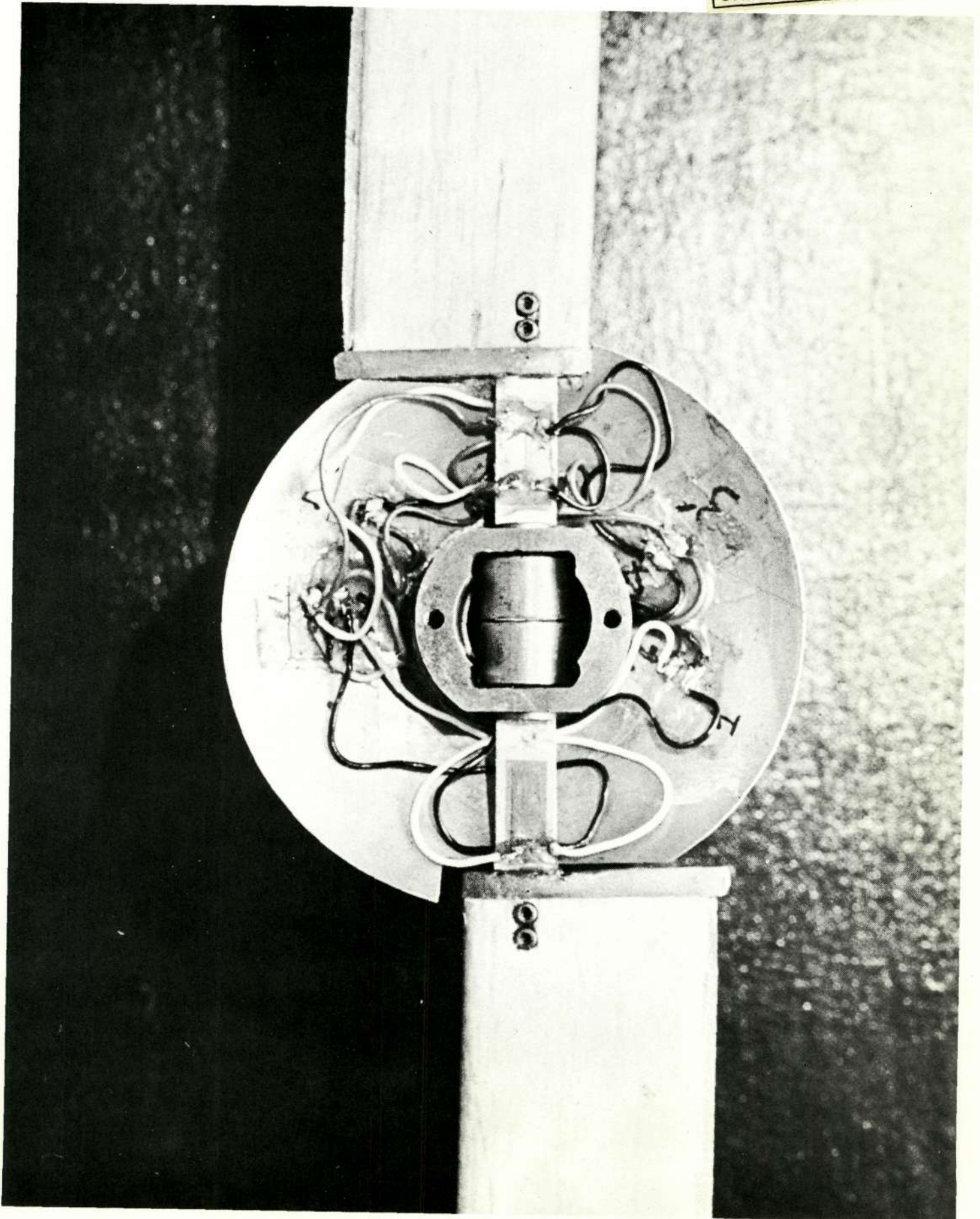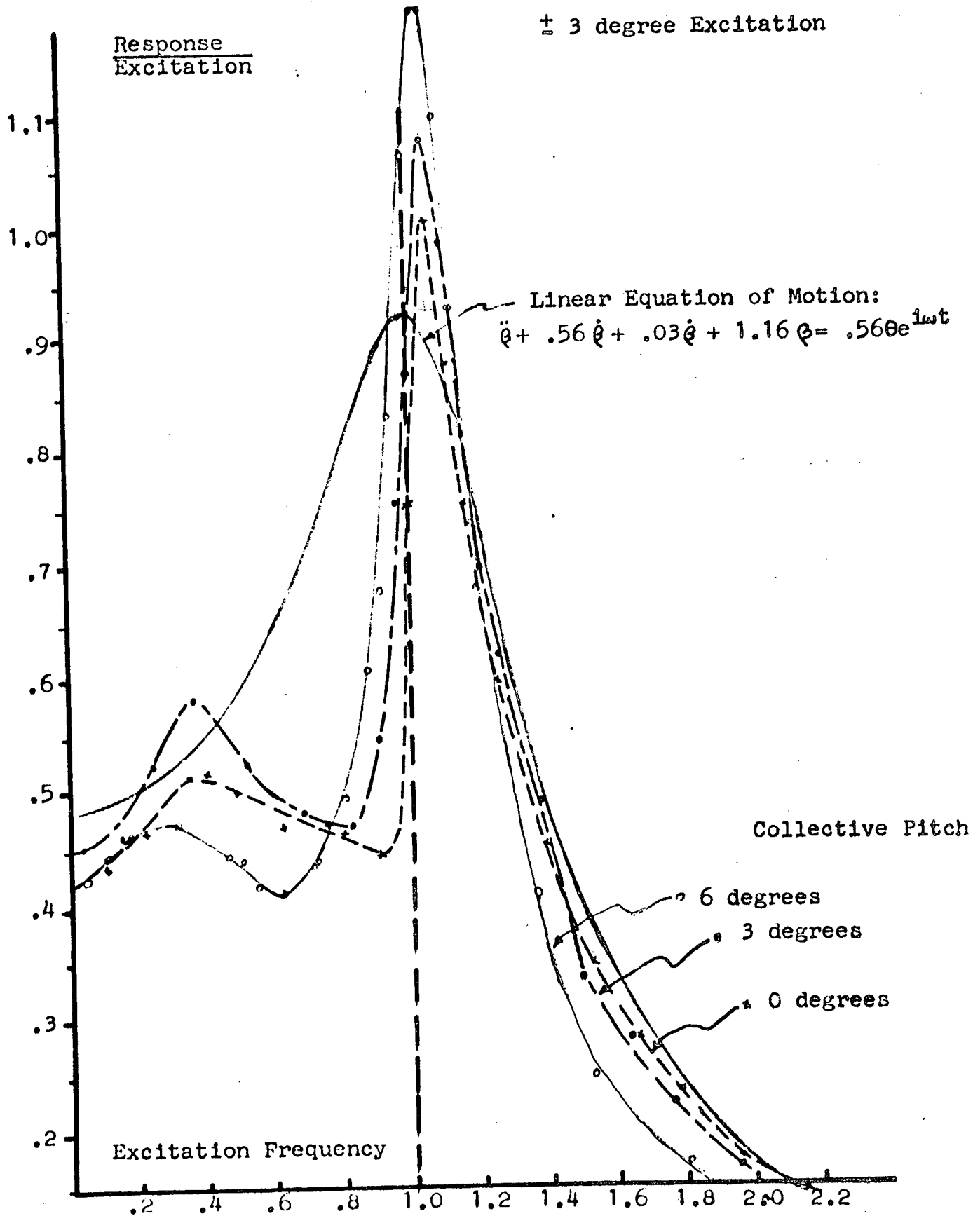
Collective Pitch

6 degrees

3 degrees

0 degrees

Excitation Frequency
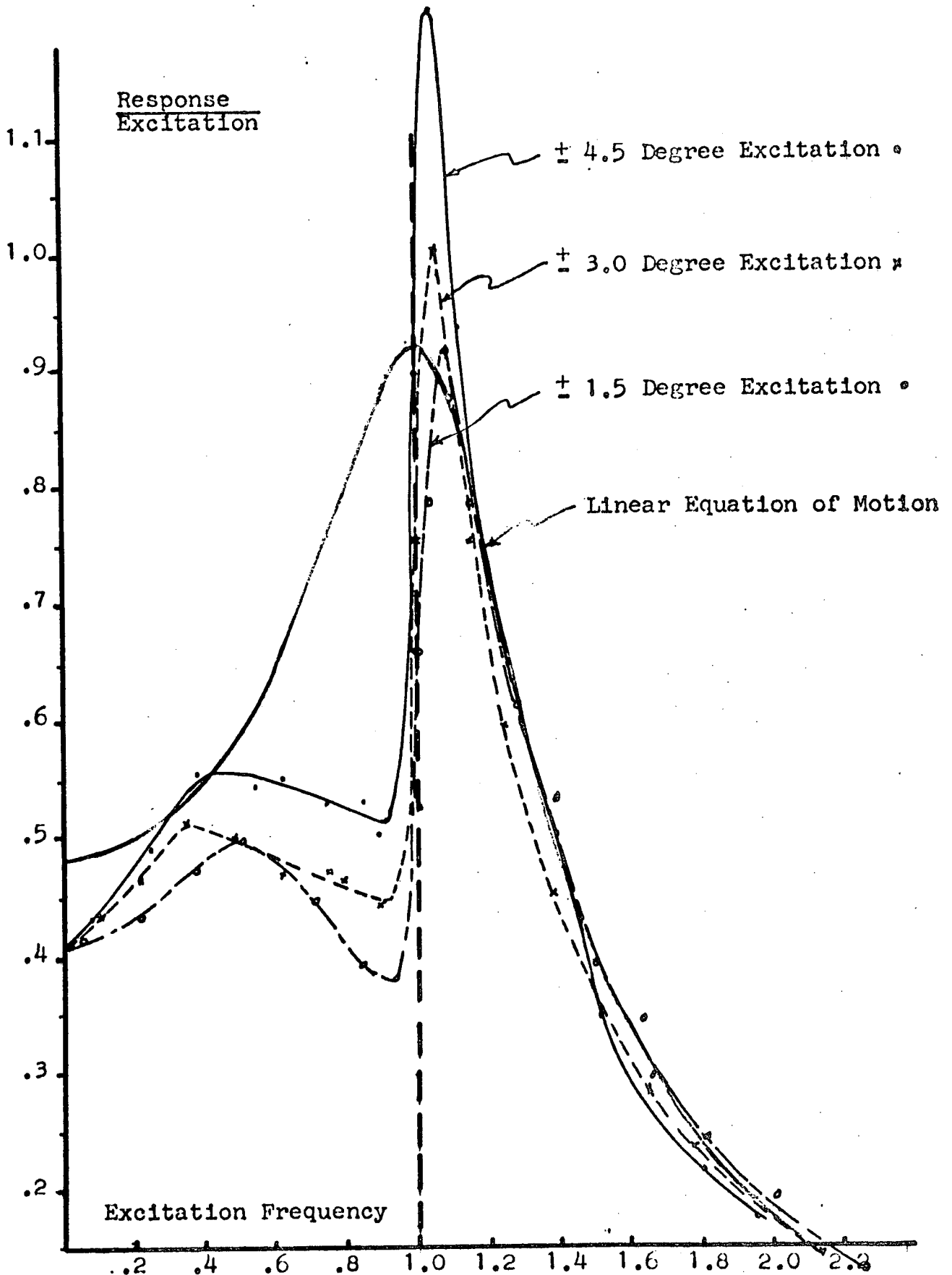
Figure B-3

Collective Pitch  0 degrees
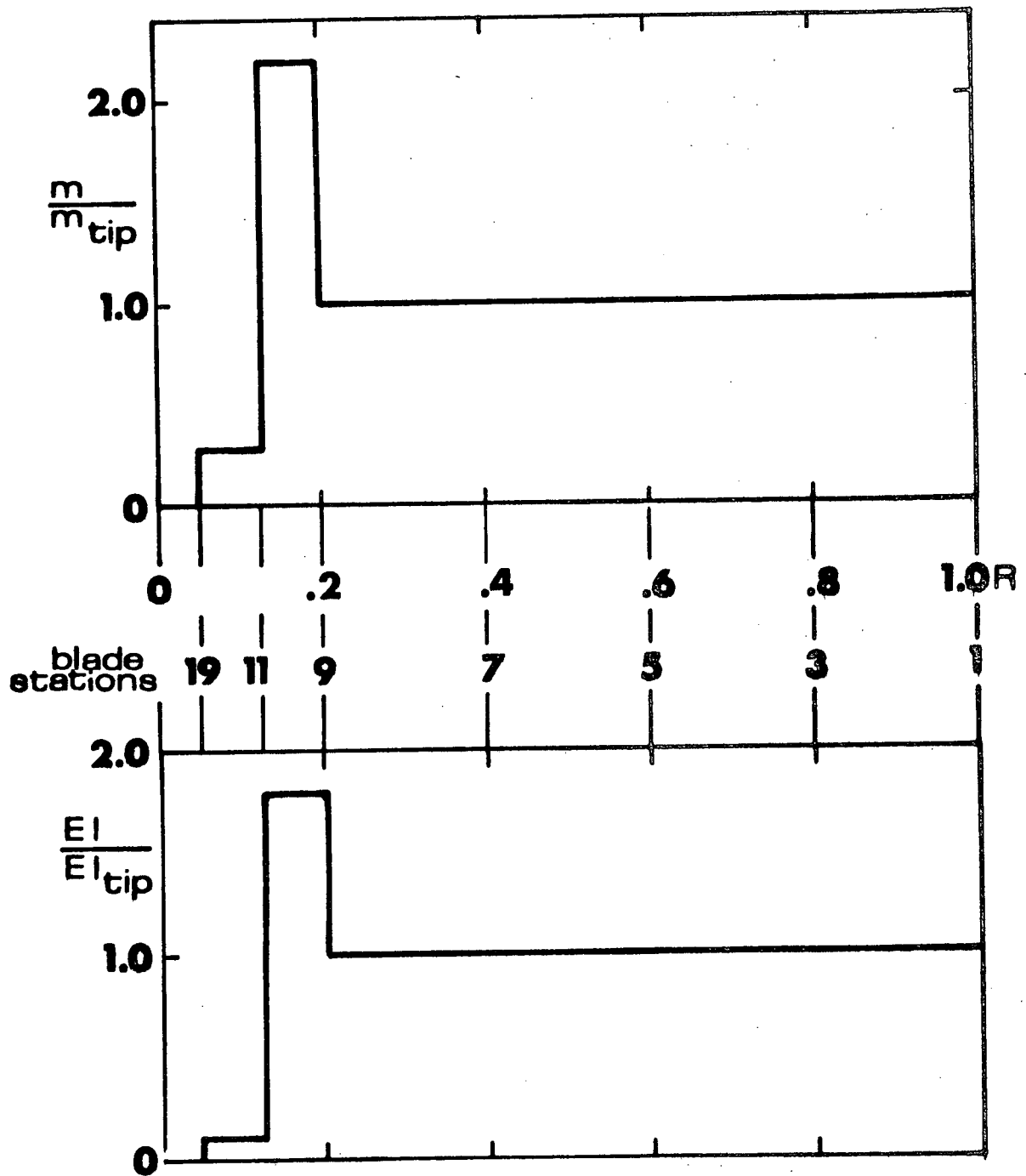
Figure B-4
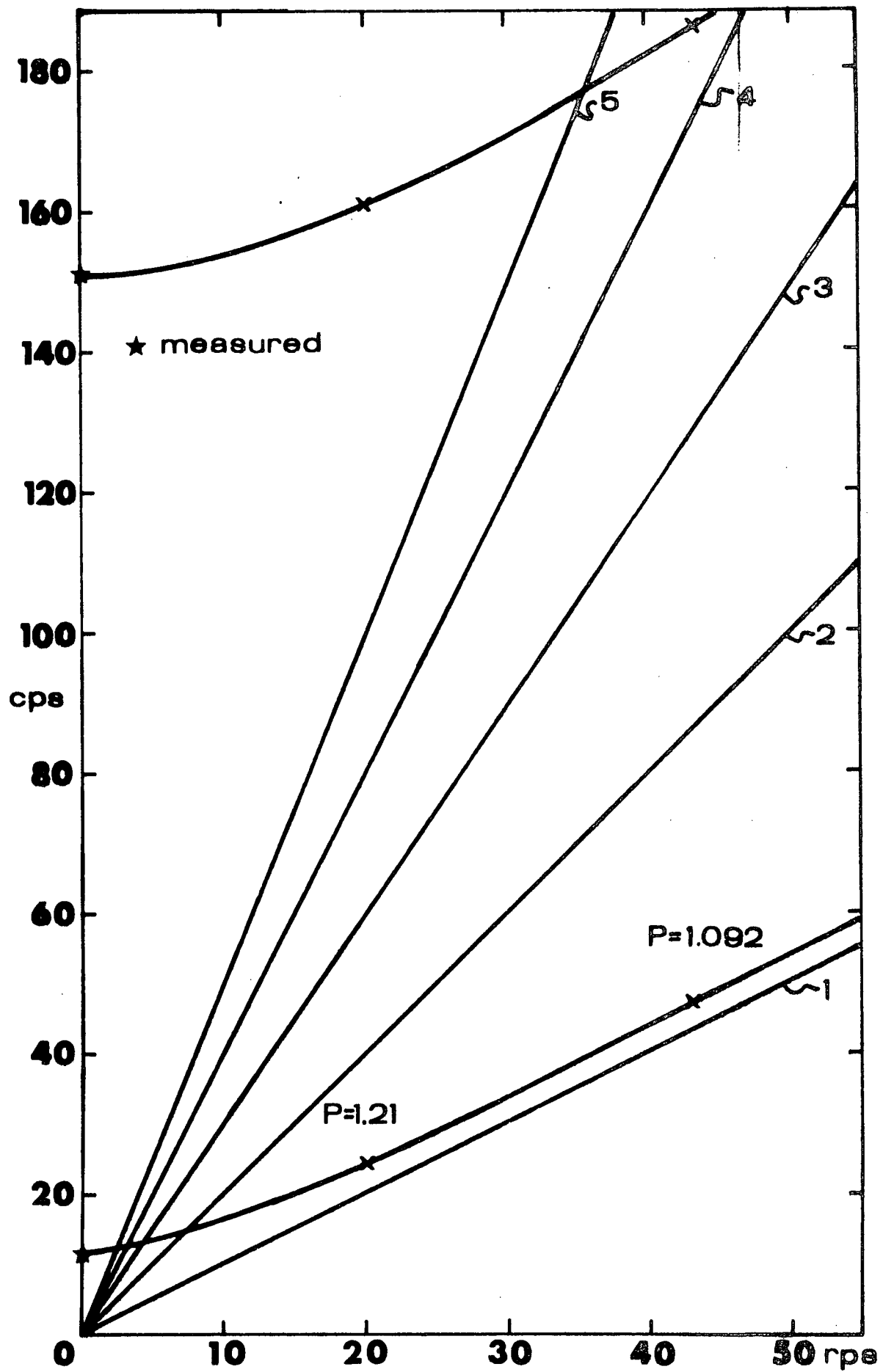
Figure B-5

Figure 6    Rotor Model

C.2.
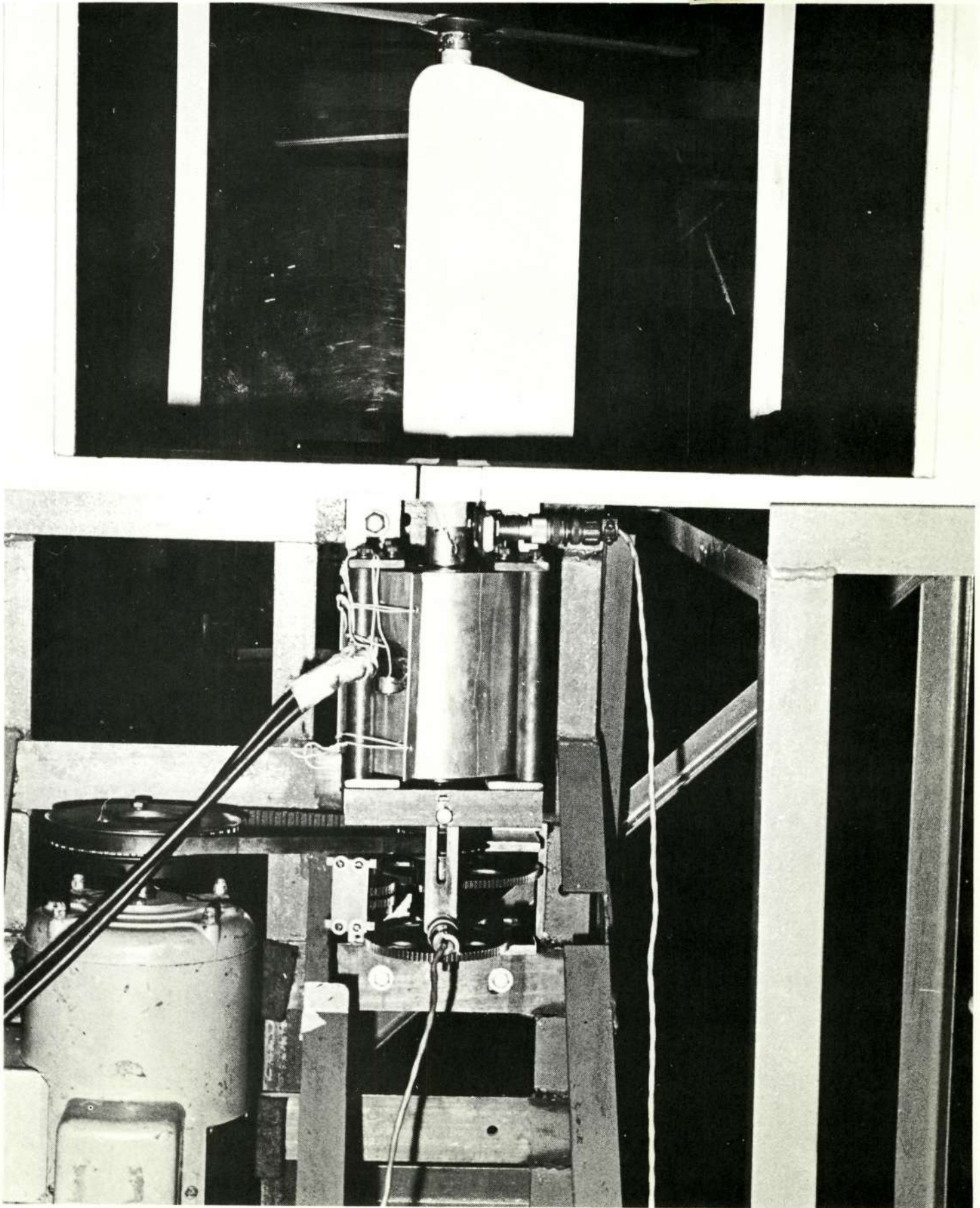
## Appendix C

## Data Processing

From the beginning of the project it was obvious that some sort of automatic data processing would be needed to analyze the large amounts of data that the model is capable of producing.

### C-1 Preliminary Hovering Data Processing

The first hovering results from the hinged model were recorded on an oscillograph which used light galvonometers (having flat frequency response characteristics form 0-600 cps) writing on light sensitive paper. Obtaining the first frequency response amplitude and phase shift characteristics, for one rotor condition (one collective pitch setting, one amplitude excitation, and approximately 20 blade cyclic pitch frequencies ranging from 0 to 2.0 times the rotor rotational speed), from these recordings by hand took 7 to 8 hours. The response to excitation frequencies between .2 and .8 P were distinctly nonsinusoidal - indicating the substantial presence of frequencies higher than the first natural frequency - therefore in this excitation range the first frequency amplitude and phase shift characteristics could only be estimated in a hand analysis. About 20 hovering rotor conditions with the hinged rotor model were evaluated in this manner. The hinged rotor model was deemed inadequate for the purpose of these experiments on

the basis of these results and subsequent damping test on
the hinges (see Appendix B). Preliminary tests on the hinge-
less rotor showed the same nonsinusoidal response charac-
teristics between .2 and .8 P indicating that even in
hovering the hand analysis is good only for seeing overall
trends. It is almost impossible to do anything by hand with
the forward flight data since in all of the forward flight
data the trim response must be eliminated.

## C-2 Testing and Analysis

The first pitch excitation system used two variable
speed motors which ran independently (see Appendix B). When
this system was designed it was thought that the model would
have to maintain the proper phasing for two or three rotor
revolutions. In a forward flight test at one rotor condi-
tion, the trim response could be found first and subtracted
from the subsequent total response to the collective pitch
plus the various cyclic pitch excitations. This approach
requires a good reproducibility of the tests including good
electronics,as the time between obtaining the trim condition
and the total responses is great,therefore making mean drift
important. Eliminating electronic mean drift over long
periods of time would require much more expensive equipment
and should be avoided if possible. Much of the automatic
data processing was designed to fit the two motor operation
and was then redesigned to fit the improved and final mode
of testing.

The final mode of testing and analysis eliminated the need for subtracting the trim response from the total response for each sample point, therefore eliminating the need for concern about mean drift. The new analysis required the pitch excitation system to maintain proper phasing for 5 to 20 rotor revolutions thus the independent motors system of pitch excitation would not do. The independent motors system of pitch excitation was, therefore, replaced by a one motor and a changeable gears system (see Appendix B).

## C-3 Signal Conditioning

To determine th rotor condition at any instant, 4 quantities were constantly monitored; rotor shaft azimuth angle, pitch shaft azimuth angle, flapping response, and torsion response (see Appendix B). The physical system used to monitor the rotor shaft azimuth angle consists of a magnetic pickup which emits a positive-negative voltage as a set screw on the rotor shaft passes through the magnetic field of the pickup. The set screw is positioned so that the blip occurs when the rotor shaft is in the zero azimuth position. The same set screw-magnetic pickup combination is used to determine the pitch shaft azimuth angle. On the pitch shaft there are two set screws 90 degrees apart. When one of these is lined up with the rotor shaft set screw, then a cosine excitation is beginning.

If the other one is lined up with the rotor shaft set screw, then a sine excitation is beginning. The physical system used to monitor the flapping and torsion response consists of strain gage bridges on the blade-hub flexures.

These four signals are recorded on an F.M. tape recorder (see Fig.C-1)and taken to a PDP-12 computer (see Fig.C-2) where they are processed. The PDP-12 is a farily new small laboratory computer, which can be operated in two modes. If it is operated in one mode, it becomes a PDP-8 which has available to it a Fortran-iv compiler, and which is very good at handling data. If it is operated in the other mode, it becomes a LINC (a laboratory computer developed at the Washington University computer systems lab), which is very good at performing input-output. The particular PDP-12 was chosen because it was usually accessible without a long wait and because it was near the experimental set-up. It belongs to the Washington University Applied Mathematics and Computer Science Department. Since there are many LINCs available at Washington University, it was decided to operate entirely in the LINC mode, in case the PDP-12 broke down for an extended period of time.

This particular PDP-12 has an 8196 twelve bit word memory, it also has two tape drives each containing 512 blocks capable of storing 256 twelve bit words. Programs are stored on tape and can be read into memory when needed. Memory can also be written on tape when necessary. For

input and program control purposes it has 16 analog-channels, eight of which can be used to accept incoming voltages from 0-2 volts and eight of which generate voltages from 0-2 volts depending on the position of a potentiometer and can be used to control a program in progress. The program can sample any one of these channels and generate a number between -512 and 512. Its output capabilities consist of a fairly fast line printer, several channels over which the program can generate voltages, and a 9 inch by 9 inch display screen capable of displaying a 512 by 512 array. The basic instruction cycle is 1.2 microseconds. All programming was done in LAP-6 machine language.

There were some minor voltage compatibility problems to overcome. The magnetic pickups generate voltages between -1 and +1 volts. It was possible to adjust the D. C. component of the tape recorder output from -.2 to +.2 volts, which is clearly not enough to raise the computer input to a 0-2 volt level, so a one volt mercury battery was inserted in a floating circuit between the tape recorder and the computer. It was also most convenient to record the flapping and torsion response in a +1 to -1 volt range in order to avoid operating in the questionable linearity ranges of both the tape recorder and the amplifiers. Therefore, an oscilloscope was inserted between the tape recorder and the computer (see Fig. 2) on the flapping and torsion response channels. The oscilloscope could then be used to add the

needed D. C. component to the signal.  The oscilloscope can also be used to attenuate the signal if necessary.

C-4 Programming

Programming was designed upon the worst possible cases (as far as memory needs go) which are the .95 and 1.05 P cyclic pitch excitations.  About 180 samples per rotor revolution are needed to identify the position of the rotor shaft and pitch shaft blips within plus or minus 1 degree. The rotor shaft makes 20 revolutions for every pitch shaft revolution at .95 and 1.05 P therefore a minimum of 3600 words of memory are needed to correctly identify the pitch shaft azimuth angle.  In forward flight these rotor excitations are periodic with 20 rotor revolutions.  Since 36 points per revolution were desired for the flapping and torsion response, each of these required a minimum of 720 words of memory.  Because of memory organization, it was most convenient to plan to take 1024 rotor shaft samples, 4096 pitch shaft samples, 1024 flapping response samples, and 1024 torsion response samples.  Rotor and pitch shaft samples are collected at the same rate.  One flapping and one torsion response sample are collected for every five rotor shaft samples.  The sampling programs occupy approximately 700 words of memory.

C-4 -1 Sampling Programs

A set of sampling programs was designed which will do

the following:

1.  Display the four quantities which are to be sampled. In this part of the sampling programs, the display screen acts as an oscilloscope with the sweep rate controlled by two of the analog potentiometers. This display allows for adjustments to be made in the D. C. components of the four signals, it also shows whether the flapping response needs attenuation.

2.  Collect the samples and put them in memory. The approximate collection starting time is chosen at the control console. The exact collection is keyed to start when it 'sees' the beginning of the first pitch blip (when the pitch blip reaches a certain voltage level). One such Sampling represents either a cosine excitation and response or a sine excitation and response. It takes two such Samplings - a cosine and a sine - to describe the general response for a particular pitch excitation.

3.  Write the Sampling on tape. The program writes the Sampling onto 32 blocks of tape, and goes back to the display segment of the program. The program will go through this cycle six times writing each Sampling onto successive blocks of tape.

C-4-2 Identification Program

After six Samplings have been taken the Identification program (1000 words) is read into memory from the control

console. The identification program reads the arithmetic
subroutines (1000 words) into memory (obtained from the
Washington University Computer Systems Lab) and then does
the following:

1. Reads the rotor shaft part of the first Sampling (1000
   words) into memory, and determines the blip locations
   and distance between blips in units of sample points.
   It does this by finding the first and last time a blip
   is below a certain voltage and averaging these four
   sample times to obtain the mean position of the blip
   which represents the zero azimuth position of the
   rotor shaft.

2. Reads the pitch shaft part of the first Sampling (4096
   words) into memory, and essentially repeats the processes
   it performed on the rotor shaft blips.

3. Looks at the pitch and rotor shaft blip positions to see
   if the Sampling is an admissible one. It will reject a
   Sampling with phasing errors greater than plus or minus
   2 degrees.

3.1. If the Sampling is admissible, the program will look
   at the relationships between the blips to see whether
   the Sampling is a cosine or a sine excitation. If
   the Sampling is a cosine Sampling, the program
   will move the flapping and torsion response to a desig-
   nated tape section. It will then see if a matching sine
   Sampling has been found - if not, it will read the rotor

shaft part of the next sampling into memory and repeat

the process until it either finds a matching sine

Sampling or runs out of Samplings to look at. If

matching sine and cosine Samplings are found the pro-

gram will read the analysis program (1000 words) into

memory.

3.2. If the Sampling is not admissible the program will look

for admissible Samplings until it finds them or until

it runs out of samples to look at.

4. If the program exhausts all the Samplings without find-

ing matching pair of cosine and sine Samplings, it will

indicate to the console whether it has found an admis-

sible cosine Sampling, or neither. The man at the con-

sole can then go back to the sampling programs and

start over.

C-4-3 Analysis Program

The analysis program (1000 words) reads the cosine

excitation flapping response (1024 words), the cosine

excitation response (1024 words), the sine excitation flap-

ping response (1024 words), and the sine excitation torsion

response (1024 words) into designated portions of the

memory. The analysis program then combines the cosine and

sine excitation rotor response to produce the generalized

rotor response to a particular cyclic pitch excitation fre-

quency. The analysis program then reads a printing and

display program into memory.

## C-4-4 Printing and Display Program

The printing and display program:

1.  Prints the results of the analysis.

2.  Saves the flapping and torsion response parts of the admissible cosine and sine Samplings on the second tape.

3.  Displays one period of the cosine and the sine excitation torsion responses.

4.  Displays the sample points of the cosine and sine excitations used in the analysis.  This display enables one to see directly if the program really integrated over one excitation period.

Processing one rotor condition takes about one to one and one half hours.

## C-5 Future Processing Improvements

The analysis program part of the processing is now the weakest link in the signal processing.  In order to keep the analysis program less than 1024 words long, which constitutes one memory bank in the computer's LINC mode, the rectangle rule was used as the scheme for integration.  The rectangle rule is good enough for finding the first harmonic but is worthless for finding higher harmonics.  It will now be replaced with Simpson's rule which will allow the second and third harmonics to be found.

The torsional moments were measured for some of the tests shown in the main part of the report. However, they have not yet been processed.
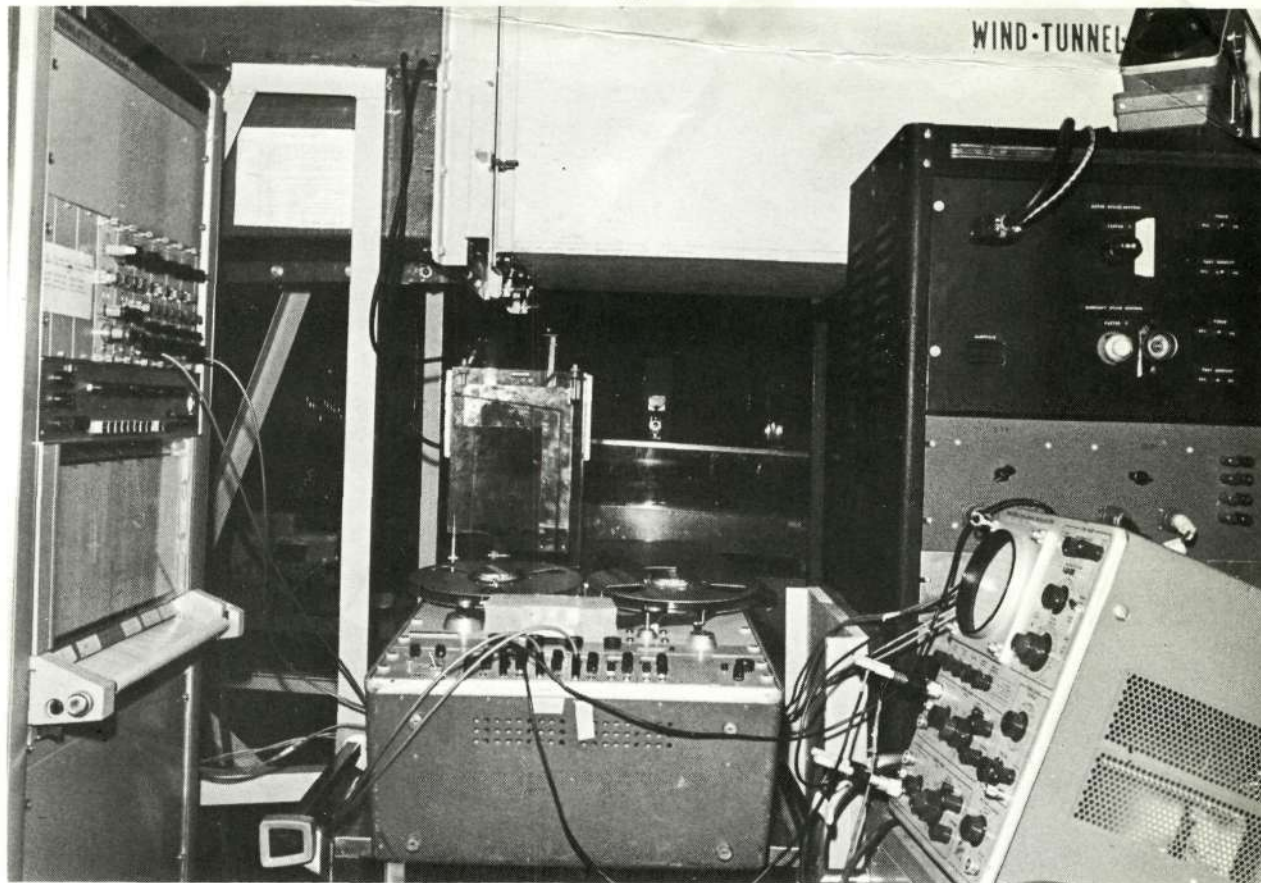
Figure I    Control and Recording Equipment

Figure 2    PDP-I2 and Playback System

## Appendix D

## List of Department Owned and Purchased Components of Test Equipment

### Department Owned

1. Eaton-Yale 1/2 H. P., 1600 rpm Adjusto speed Motor, #5041           New Value . . . . . $  275.00

2. Tektronix Type 502A Dual Beam Oscilloscope

    New Value . . . . . $1,100.00

3. Ampex FR-1300 Recorder/Reproducer

    New Value . . . . . $7,500.00

4. Hewlett Packard Thermal Recording System 7706B

    New Value . . . . . $7,500.00

5. Consolidated Electrodynamics Corporation Type 5-124 Recording Oscillograph

    New Value . . . . . $3,000.00

6. 2 channel adjustable high-low pass variable filters

    New Value . . . . . $2,200.00

7. Simpson Circuit Tester

    New Value . . . . . $  140.00

8. Hewlett Packard Audio Oscillator

    New Value . . . . . $  340.00

### Purchased

1. Airelyte Electronic Co. Type CAY-125-12 Slip Ring and Brush Block Assemby

    Price . . . . . . . $  470.00

2.  One Eaton Yale Adjustospeed Motor, Model #5021

                            Price . . . . . . . $ 272.86

3.  One Hewlett Packard 8802A medium gain D. C. amplifier

                            Price . . . . . . . $ 325.00

4.  3 Consolidated Electrodynamics 7-323 galvonometers

                            Price . . . . . . . $ 360.00